Balancing the Intermolecular Forces in Peptide Amphiphiles for pH-Triggered Self-Assembly

Undergraduate Honors Research Thesis

Presented in Partial Fulfillment of the Requirements for graduation "with Honors Research Distinction in Chemistry" in the Arts and Sciences of The Ohio State University

By:
Michael J. Nicholl

The Ohio State University
December 2014

Honors Defense Committee:

Professor Joshua Goldberger (Project Advisor)

Professor Jonathon Parquette

Professor Harald Vaessin

Table of Contents

Acknowledgements

Special thanks are extended to Dr. Arijit Ghosh and Christian Buettner for their contributions to the advancement of this project. Further thanks to Dr. Ghosh for his teaching and advisement throughout this process. To Dr. Elizabeth Hommel and Dr. Marina Bakhtina, thank you for your training and support with the use of the Electrospray Ionization Mass Spectrometer and Jasco Circular Dichrosim Spectrometer. Thank you to The Ohio State University Department of Chemistry and Biochemistry for their dedication and commitment to undergraduate research and education. Lastly, thank you to my advisor Dr. Josh Goldberger for providing me with the opportunity to conduct research in your lab and your continued guidance for the past two years. It has truly been a fantastic experience.

Vita

Education:

Warren G. Harding High School……...……2010
-Diploma

The Ohio State University……...……..…2014
-B.A. Chemistry
-Minor: Biology
-Magna Cum Laude

Honors and Awards:

- Midwestern Symposium on Undergraduate Research in Chemistry Best Materials Poster (2014)
- Univ. Texas Southwestern McKnight Chemistry Award Semifinalist (2014)
- Ohio State Mayers Summer Undergraduate Research Fellowship (Summer 2013)
- Gary Booth Chemistry Scholarship (2013-2014)
- Scarlet and Grey Scholarship (2012)
- The Ohio State University Honors Program (2011-Present)

Publications:

- A. Ghosh, E. T. Dobson, C. Buettner, M. Nicholl, J.E. Goldberger, "Programming pH-Triggered Self-Assembly Transitions via Isomerization of Peptide Sequences." Submitted

Abstract

The design of novel self-assembling biomaterials that change morphology in response to specific stimuli can lead to much advancement in designing next generation sensors, diagnostic and therapeutic agents. We have previously developed a new class of self-assembling materials known as peptide amphiphiles (PA) that transform from spherical micelles to nanofibers in the slightly acidic environment of cancerous tissue, as a novel mechanism to enhance their accumulation at the tumor site relative to normal tissue. A typical PA that we construct consists of an alkyl tail, followed by an amino acid sequence, and terminated with a MRI imaging agent. However, designing this vehicle that will transform under a specific pH value *in vivo* requires a more detailed understanding of the relative attractive hydrophobic and the repulsive electrostatic forces in these surfactant-like molecules. Here, we specifically studied how the alkyl chain length, the number of anionic amino acids in the molecule's charged region, and the number of tyrosine (Y) residues in the its beta sheet region affect the sphere to nanofiber transition pH, starting from palmitoyl-YYAAEEEEK(DO3A:Gd)-NH_2. In general, it was shown that increasing the alkyl chain length promotes nanofiber formation under a given set of conditions, while increasing the number of charged amino acids promotes micelle formation. Furthermore, it was determined that the addition of a fifth glutamic acid shifts the pH of the sphere to nanofiber transition to a slightly more acidic value as compared to the deletion of a single methylene group or tyrosine residue.

Chapter 1: Introduction

Cancer is one of the most prevalent diseases in the world, accounting for over 8.2 million deaths worldwide in 2012[1]. The World Health Organization (WHO) estimates that the number of annual cancer cases will rise by 8 million in the next twenty years[2]. With these staggering statistics, there is much interest in the biomedical community to develop new methods of treating and detecting cancer. For example, the development of new biomaterials for drug delivery via the recognition of specific biomarkers in cancer has received much attention for its targeted therapeutic effects[3-7]. There is also an interest in the development of stimuli responsive molecules for the detection and treatment of cancer, in order to better pinpoint the location of a tumor in the body to have enhanced treatment of the disease[8-11]. One stimuli that is currently be explored is the slightly acidic microenvironment around the leaky vasculature of tumor tissue, due to a cancer cells increased rates of glycolysis[12]. The pH for this area ranges from 6.6-7.2; slightly depressed from the normal physiological pH of 7.4[12]. By exploiting this characteristic, new methods of cancer imaging and therapy can be developed to better enhance a patients quality of care.

In the Goldberger Group, we are designing and characterizing a new class of stimuli responsive self-assembling molecules called Peptide Amphiphiles (PAs) to be used for cancer imaging purposes. PAs are of much interest because of their ability to exist as a single molecule, spherical micelle or cylindrical nanofiber depending on their concentration and the pH of the environment. We have designed these molecules in such a way that they have the ability to undergo a pH-triggered morphological transition from a micelle to a nanofiber in a slightly acidic environment that parallels to that of a tumor[13]. This transition is vital in order for these

molecules to have enhanced accumulation at the site of the tumor. **Figure 1** shows the overall goal and mechanism of these molecules, achieved by a sphere to nanofiber transition in the presence of a particular stimulus, specifically the acidic environment of a cancerous tumor.

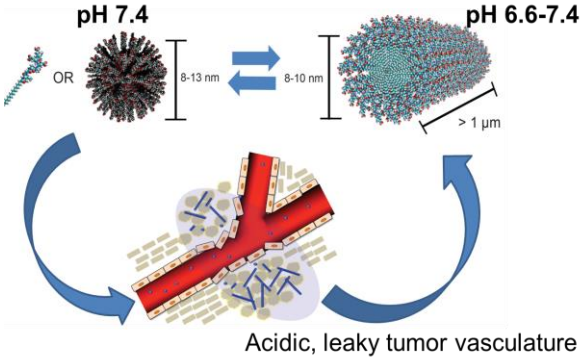

Figure 1: Schematic representation of sphere to nanofiber transition around a malignant tumor.

The ability for the PA to exist as a sphere or a nanofiber is essential to our overall goal of creating a dynamic self-assembling, stimuli responsive imaging agent. By having these molecules in a micellular morphology, one can exploit the enhanced permeation and retention (EPR) effect[14] as a method of having our material diffuse into the cancerous environment due to the permeable blood vessels that exist around the tumor site[15]. This effect depends on the molecule's characteristics that include size (typically 10-30 nm in diameter), zeta potential, biocompatibility and solubility[14]. In order to accomplish this effect, the engineering and design of these PAs requires much attention.

A typical PA consists of an alkyl tail, followed by an amino acid sequence, and terminated with a MRI imaging agent (**Figure 2**). The amino acid sequence contains a hydrophobic beta-sheet forming region, followed by an electrostatic charged region. The MRI region consists of a Gd^{3+} chelated 1,4,7- tris(carboxymethylaza)cyclododecane-10-

azaacetylamide (DO3A) moiety to allow the molecules to be MRI active[16-18]. Both the alkyl tail and the beta-sheet region promote nanofiber formation, while the charged region promotes micelle morphology. All four of these regions (including the MRI region), have an effect on the self-assembly properties of the PAs. The design of the PAs is such that the EPR effect can be obtained. The negatively charged region allows for the zeta potential to be less than zero, while the hydrophobic regions allow for slightly decreased solubility, both of which are important for the EPR effect. Also, since these molecules are peptide-lipids, both of which have high compatibility within the body, these molecules will be non-cytotoxic. The size of our PAs existing in a micelle morphology has been shown to be 10.0 ± 1.2 nm[13] which is in the range in which the aggregated molecules can easily diffuse into malignant area and the EPR effect can take place[14].

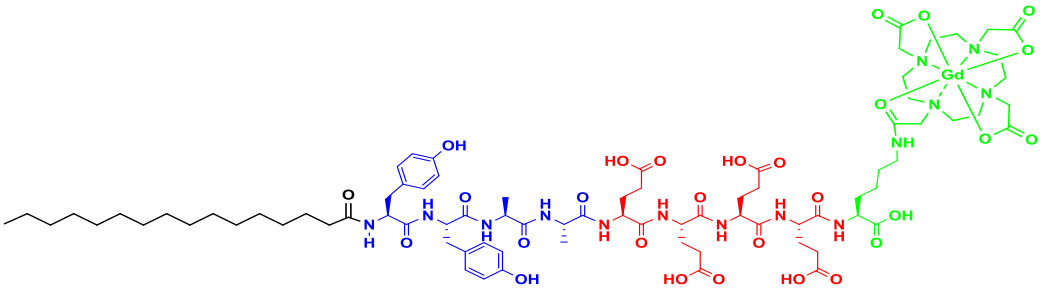

Figure 2: Synthesized PA with alkyl tail (black), beta-sheet region (blue), charged region (red) and MRI region (green). This PA is palmitoyl-YYAAEEEEK(DO3A:Gd)-NH_2.

By balancing the attractive hydrophobic and repulsive electrostatic forces in these molecules, one could design a vehicle that transforms from a sphere to a nanofiber at a specific pH *in vivo*. However, designing PAs to undergo this pH-specific transition requires a more detailed understanding of the PA's relative forces, and their impact on the self-assembling

properties of these surfactant-like molecules. To these ends, we have synthesized and characterized four different PAs to test how certain structural changes affect the molecule's supramolecular characteristics. We focused on the alkyl chain length, the number of glutamic acids (E) in the charged region and the replacement of a tyrosine (Y) residue by an alanine (A) in the beta-sheet region to determine how changes to these areas of the PA affect the sphere to nanofiber transitional pH as well as the molecule's ability to exist as three district morphologies. These PAs include palmitoyl-YYAAEEEEK(DO3A:Gd)-NH_2 (PA1), palmitoyl-YYAAEEEEEK(DO3A:Gd)-NH_2 (PA2), pentadecyl-YYAAEEEEK(DO3A:Gd)-NH_2 (PA3), and palmitoyl-YAAAEEEEK(DO3A:Gd)-NH_2 (PA4). Through different analytical techniques and characterization methods, phase diagrams were able to be constructed for each of the synthesized molecules. From this, we have a more detailed understanding of how particular changes to these molecules affect its morphology at differing concentrations and pH values.

Chapter 2: Construction of Phase Diagrams

All of the PAs for this project were synthesized via solid-phase Fmoc chemistry[19] and purified by reverse-phase high performance liquid chromatography (HPLC). Their purity was determined by analytical HPLC and electrospray ionization time-of-flight mass spectrometry (ESI-TOF MS) (**Figures S1-2**).

The first PA synthesized was palmitoyl-YYAAEEEEK(DO3A:Gd)-NH_2 (PA1). Because of the two neighboring tyrosine (Y) residues in the beta-sheet region, it was thought that this PA would self-assemble into a nanofiber relatively easily (at higher pH values) due to tyrosine's high beta-sheet propensity[20-21]. Circular dichroism (CD) spectroscopy was employed in order to determine the morphology of the PA at differing concentrations and pH values[22]. For CD measurements, the PA was placed in a 150 mM NaCl, 2.2 mM $CaCl_2$ simulated serum salt solution. For PA1, it was found at a wide range of concentrations and pH points, the CD spectra showed a beta-sheet curve, one of three readout that are observed in CD[22]. Spectras of PA1 at concentrations of 500 μM and 10 μM, with pH values ranging from 11 to 5 conclude the molecule exists as a single morphology by only yielding only a beta sheet curve. **Figure 3** shows the beta-sheet curve for PA1 at 10 μM over a wide pH range. The beta-sheet curve via CD is indicative of a self-assembled nanofiber species, which was confirmed by transmission electron microscopy (TEM) of the 500 μM sample (**Figure 3 b&c**).

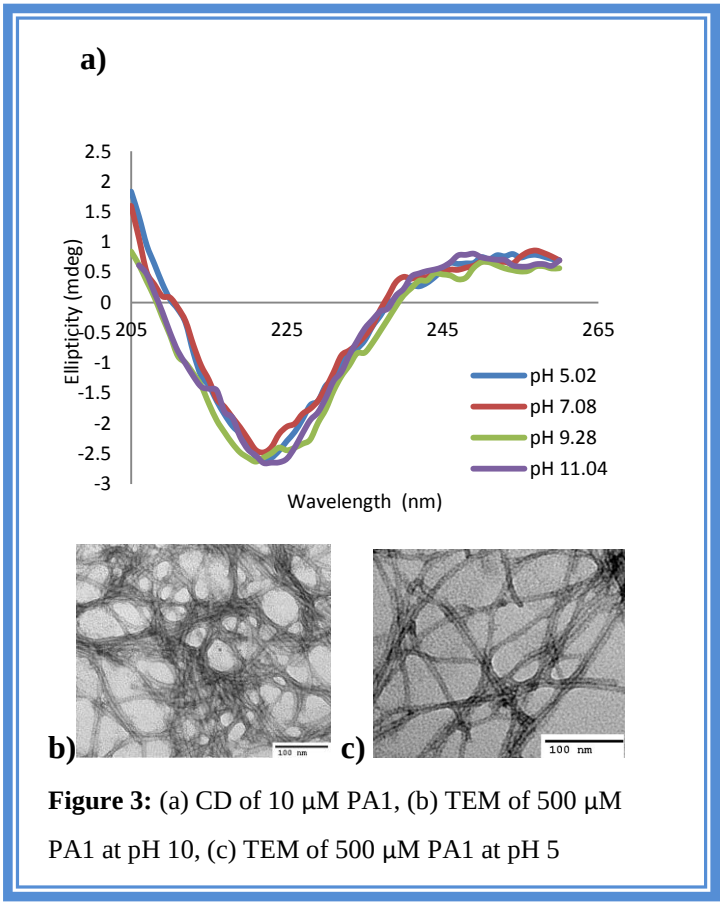

Figure 3: (a) CD of 10 μM PA1, (b) TEM of 500 μM PA1 at pH 10, (c) TEM of 500 μM PA1 at pH 5

The next step in this project was to move forward from the results observed for PA1 to construct PAs that will have decreased hydrophobic interactions or increased electrostatic repulsions. The hypothesis put forth was by taking either of these two avenues, the synthesized PA would exist as a micelle or single molecule, and undergo a transition to a nanofiber at decreased pH values. Both of these structural changes would lead to the synthesized PA to have a lower affinity to self-assemble into a nanofiber morphology, thus giving it a higher chance to exist as a micelle or single molecule depending on its concentration and the pH of the environment.

With this in mind, palmitoyl-YYAAEEEEEK(DO3A:Gd)-NH_2 (PA2) was synthesize, thus increasing the relative electrostatic repulsions by adding an additional glutamic acid (E) to the charged region as compared to PA1. As a consequence, it was expected that the PA would exist as an alternative morphology, such as a micelle or single molecule, as compared to only being a nanofiber observed with PA1. This hypothesis is due to the increase in the electrostatic repulsive forces of PA2, thus making it more difficult to self-assembly into a nanofiber. This was confirmed via CD, as it was shown that a transition from a random coil spectrum to a beta-

sheet spectrum occurred when the pH was lowered to a more acidic value. We attribute the random coil spectrum to be indicative of a single molecule or spherical micelle.

From this, we were able to obtain an approximate pH of morphological transition from a micelle or single molecule to a nanofiber by taking the midpoint between the lowest pH value of a random coil spectrum and the highest pH value a beta-sheet spectrum. For example, at 50 μM for PA2 (**Figure 4a**), we see the last random coil spectrum (where the y-intercept at 205 nm is negative) at a pH 5.80. We then see the first beta-sheet spectrum (where the y-intercept at 205 nm is positive) at a pH of 5.69, giving an approximate pH of transition at a value of 5.76. This same process was carried out at 500 μM, 100 μM, and 30 μM.

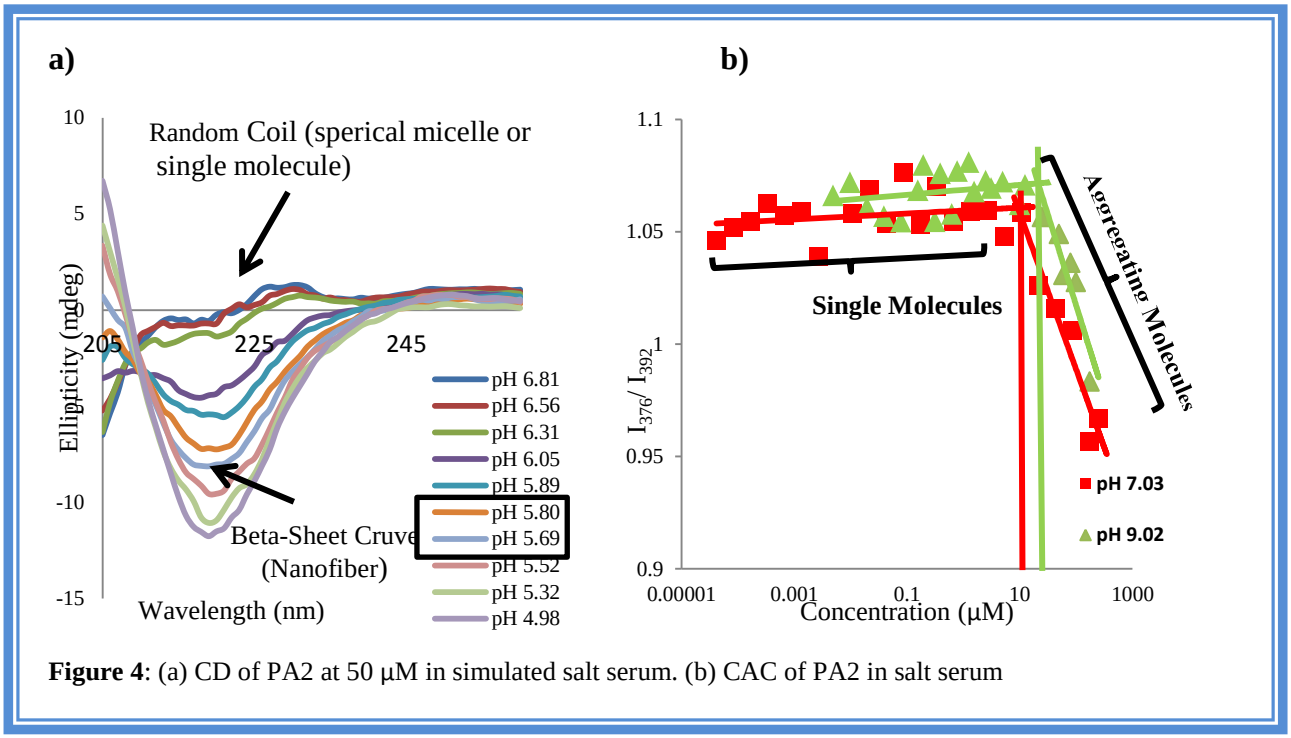

Figure 4: (a) CD of PA2 at 50 μM in simulated salt serum. (b) CAC of PA2 in salt serum

Since a random coil spectrum can correspond to a single molecule or a micelle, critical aggregation concentration (CAC) was employed in order to not only distinguish between these two morphologies, but also determine at what concentration PA2 aggregates at a particular pH.

CAC measurements for PA2 were carried out using the pyrene 1:3 method[23] at pH values of 9, 8, 7, 6 and 5. It was observed that at acidic pH values, the CAC was at a lower than at a more basic pH. This aligns with the hypothesis that the PA will have a higher affinity to aggregate at lower pH values. For example, **Figure 4b** shows how the CAC at a pH of 9 and 7 compare, as the CAC pH 7 was calculated to be 9.37 μM, while at pH 9 the CAC is 21.59 μM. This is due to the protonation of the carboxylic acids present in the glutamic acid residues and DO3A moiety, leading to decreased electrostatic repulsions at a lower pH.

From CD and CAC, a phase diagram was able to be constructed detailing PA2's morphology at a given pH and concentration value (**Figure 5a**). From this we can see a concentration dependence on the pH of transition from the CD, as well as pH dependence on the CAC value. Once the phase diagram was constructed, confirmation was needed to show PA2's distinct morphologies. TEM was used to show nanofiber formation of 500 μM PA2 at pH 5 and micelle formation at the same concentration at pH 9 (**Figure 5b&c**).

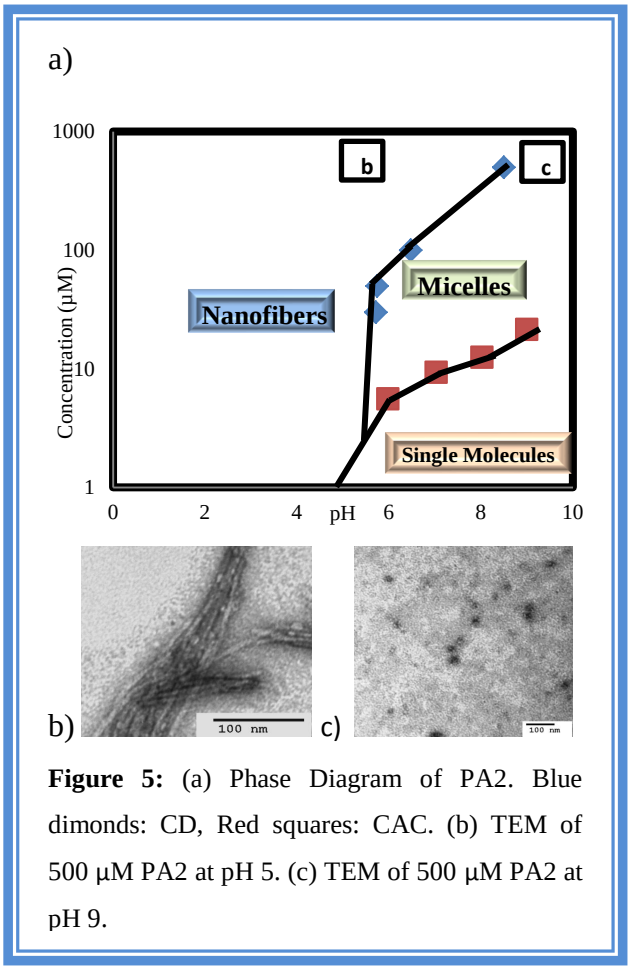

Figure 5: (a) Phase Diagram of PA2. Blue dimonds: CD, Red squares: CAC. (b) TEM of 500 μM PA2 at pH 5. (c) TEM of 500 μM PA2 at pH 9.

The second structural change that we made to the PAs, in comparison to PA1, was to decrease the attractive forces present in the molecule rather than increasing the electrostatic forces seen with PA2. The first

way that we accomplished this was by using a pentadecylic acid ($C_{15}H_{30}O_2$) lipid acid as opposed to palmitic acid ($C_{16}H_{32}O_2$) for the hydrophobic alkyl tail to synthesize pentadecyl-YYAAEEEEK(DO3A:Gd)-NH_2 (PA3). The deletion of a single methylene (-CH_2) group from the alkyl chain was thought to again give PA3 the ability to exist as different morphologies rather than only as a nanofiber.

At 500 μM, CD shows PA3 solely as a nanofiber by only showing a beta-sheet spectrum at a wide range of pH values. However at 100 μM, a random coil spectrum shows at elevated pH values a transition to a beta-sheet spectrum occurs at a pH 7.10 (**Figure S3**). With the CD measurements for PA3 at concentrations at 100 μM or less, the beta sheet curve never crossed the x-axis, even though there was a minimum at 220 nm (**Figure S3**). This shows of possible mix of morphologies[24]. However, we attributed the pH of transition to be the midpoint at which the curves no longer superimposable. CAC were carried out on PA3 in the same way as PA2 and another phase diagram was able to be constructed (**Figure 6a**). The nanofiber and micelle morphologies at 100 μM were confirmed by TEM, with clear and visible images (**Figure 6b&c**).

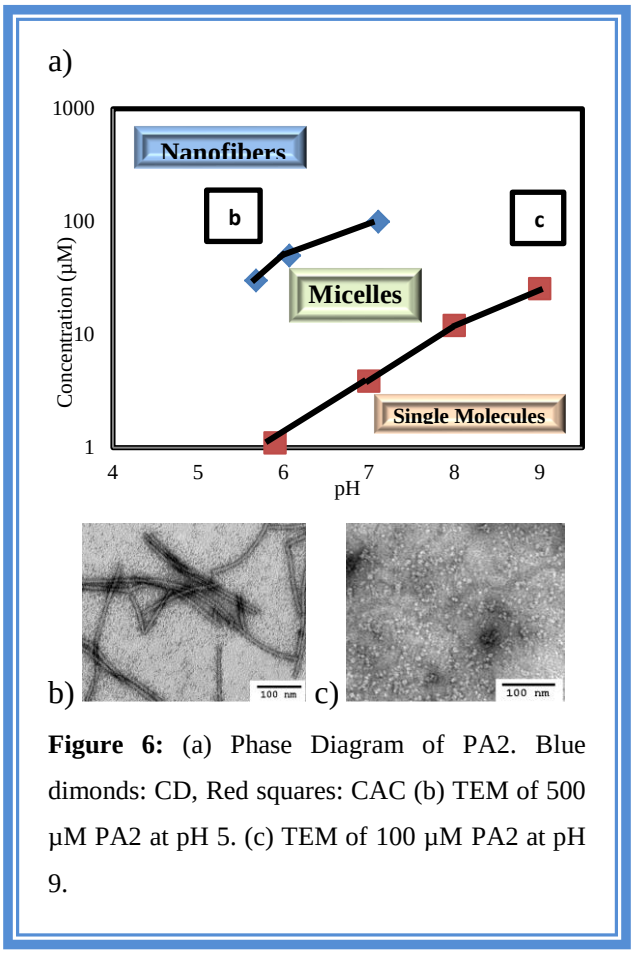

Figure 6: (a) Phase Diagram of PA2. Blue dimonds: CD, Red squares: CAC (b) TEM of 500 μM PA2 at pH 5. (c) TEM of 100 μM PA2 at pH 9.

Recently, a third structural change was carried out which parallels the decrease in the relative attractive forces relative to PA1. palmitoyl-YAAAEEEEK(DO3A:Gd)-NH_2

(PA4) was synthesized in order to decrease the beta sheet propensity of the molecule by replacing the second tyrosine (Y) residue with an alanine (A) residue in the beta-sheet region of the PA. Again, by decreasing the attractive forces as compared to PA1, PA4 will have a lower affinity to self-assemble into a nanofiber. The ratio of one highly hydrophobic amino acid, in this case Y, to three A residues, to four E residues has been a typical PA sequence for past research in our group[13], which is another reason why we wanted to test the self-assembly profile of PA4. As with the other molecules, CD and CAC were carried out of PA4 to construct a third phase diagram (**Figure 7**). However, more CD points need to be examined in this molecule to have a more complete phase diagram.

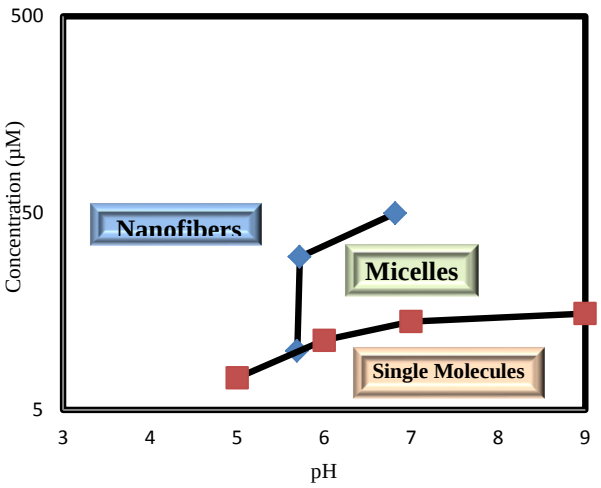

Figure 7: Phase diagram of PA4. Blue dimonds: CD, Red squares: CAC

Chapter 3: Comparison of PAs

Circular Dichroism:

By comparing Circular Dichorism (CD) measurements of the four synthesized PAs, we are able to see the differences in their respective sphere to nanofiber transitional pH. This transition is vital for the development of the imaging vehicle we are engineering. It is to be expected that our molecules will exist as a micelle at physiological pH and a nanofiber in slightly acidic surroundings. Because of this change in morphology, the sphere to nanofiber transition is closely examined for the future direction of this project.

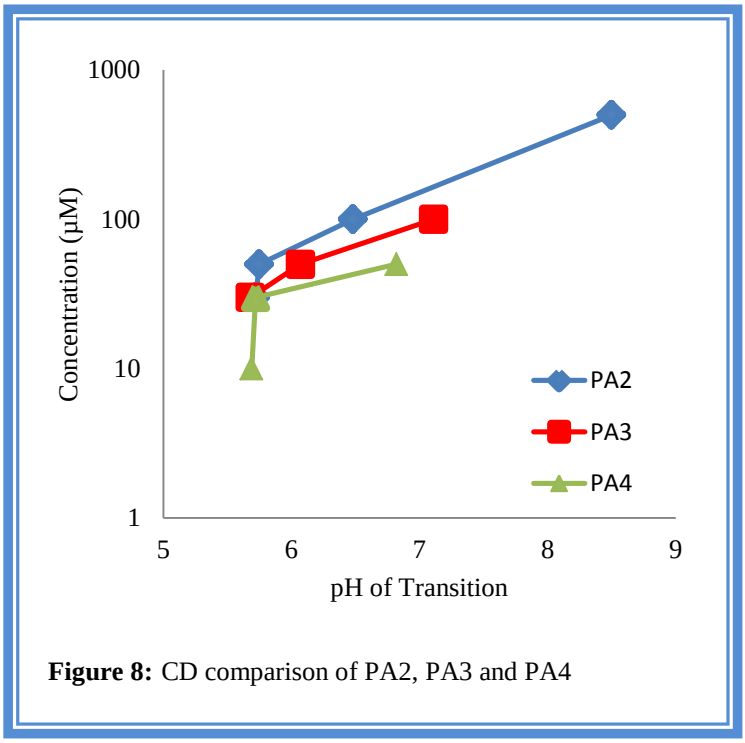

Figure 8: CD comparison of PA2, PA3 and PA4

For PA1, there was no observable transition noted from the CD, showing only a beta-sheet curve at a wide range of concentrations and pH values. Again, this readout is indicative of a nanofiber morphology, and was confirmed by TEM. However, we do see sphere to nanofiber pH dependent transitions present in PA2, PA3, and PA4, showing that structural changes from

PA1 allow the molecule to undergo a transition, and not remain as a single morphology. **Figure 8**, shows the CD transitional pH points for the three molecules at different concentrations.

From this data, we see that for all of the tested PAs, there is a concentration dependence on their pH of transition. This is noted by the more basic transition pH values especially in concentrations greater than 30 μM within each respected data set. All three of the PAs with transitions show very similar transitional pH values at 30 μM, all being within 0.03 pH units of one another, showing possible continuity of the molecules at lower concentrations. We have seen this concentration dependence in past PAs that do not have the DO3A:Gd tag attached. However, in palmitoyl-IAAAEEEEK(DO3A:Gd)-NH_2, there is very little effects of the concentration on the pH of transition[13]. Ideally, this is what we are looking for in a delivery vehicle, a PA that will transition at or around the same pH regardless of its concentration. This concentration dependence could be attributed to the tyrosine residue(s), as the aromatic and the free hydroxyl group could lead to extra pi-pi interactions and hydrogen bond interactions respectively.

PA2 shows transitional pH points that are shifted to more acidic values in comparison to PA3 and PA4. For example, at 50 μM, PA2 has a sphere to nanofiber transition at pH 5.75, a more acidic value compared to the transitional pH of 6.07 in PA3 and 6.82 in PA4. Also, we see a transition at 500 μM for PA2 that we do not see in PA3. This shows that the addition of a fifth glutamic acid to the charged region better allows the molecule to exist as a micelle at higher concentrations as compared to the deletion of a single methylene group, and possibly (due to the lack of present data), the exchange of a tyrosine residue to an alanine residue. To recall, PA3 shows only a beta sheet curve at 500 μM, meaning at higher concentrations it exits as a nanofiber.

Furthermore, it was discovered that PA4 shows the most basic transitional pH points in comparison to PA2 and PA3 at 50 μM. This data shows that the changing of the second tyrosine residue to an alanine does not have as great an effect of the pH of transition as compared to addition of a fifth glutamic acid (PA2) or the deletion of a methylene group (PA3). Since PA1, PA2 and PA3 have a beta sheet region that follows the sequence -YYAA- the two neighboring tyrosine residues could have interactions with one another, thus making the intermolecular interactions slightly decreased due to these intramolecular interactions, making it more difficult to assemble. The exception would be PA1 because of the lack of high repulsive forces and the presence of the palmitic acid tail. However, in PA4, the beta sheet region has the sequence -YAAA-, not allowing for the possible intramolecular interactions which would lead more intermolecular interactions. These increased intermolecular interactions could be the reason as to why PA4 self-assembled easier, or at a higher pH.

Critical Aggregation Concentration:

Through the comparison of Critical Aggregation Concentration (CAC), we are able to see how each respective molecule's affinity to form a micelle from a single molecule compares to others. These measurements are important for the future of this project as it tells us at what concentration our molecules need to be when injected into a test mouse. We want theses PAs to exist as micelles at physiological pH and knowing what the CAC is for the molecule at that value (pH 7.4) as well as other values is important for the development of new PAs and phase diagrams. **Figure 9** shows the comparison of the CAC measurements of PA2, PA3 and PA4.

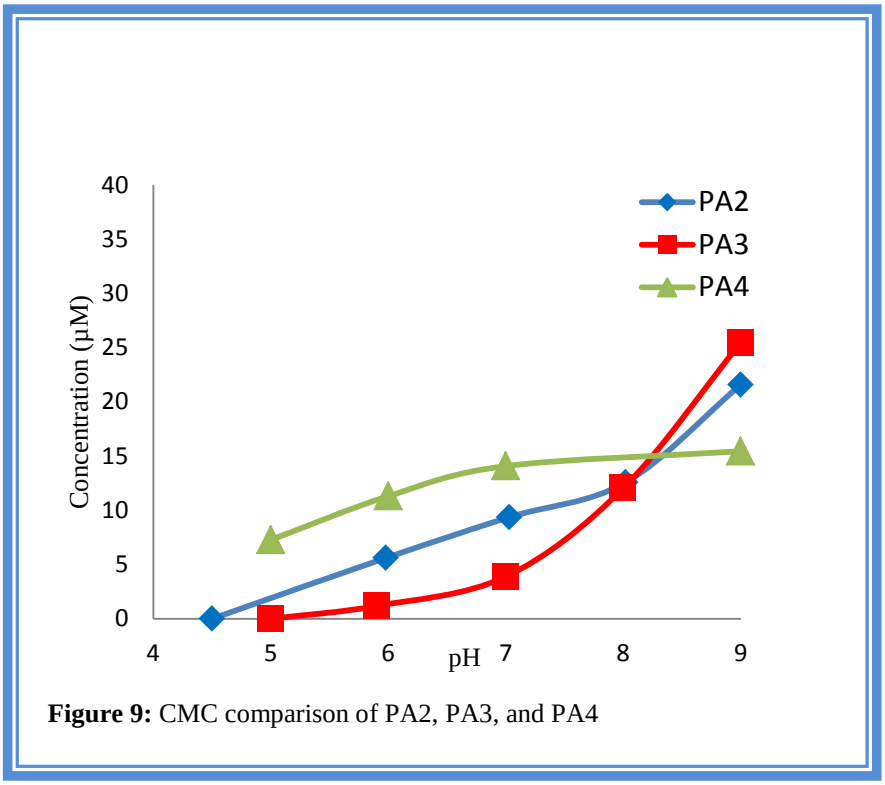

Figure 9: CMC comparison of PA2, PA3, and PA4

From this data, we see at acidic, neutral, and slightly basic conditions, PA4 has a higher CAC compared to PA2 and PA3. For example, at a pH of 7, PA4 has a CAC of 14.08 μM, while PA2 and PA3's CAC correspond to 9.37 μM and 3.89 μM respectively. This shows that at these pH values, PA4 has a lower affinity to self-assemble into a micelle as compared to PA2 and PA3, meaning that it more prefers to be in a single molecule morphology. This can be attributed to the decreased attractive hydrophobic interactions of PA4 due to only having one tyrosine residue, while PA2 and PA3 have two tyrosine residues. The heightened hydrophobic forces allows PA2 and PA3 to self-assemble more easily (at lower concentrations) as compared to PA4 with a decrease in the relative hydrophobic interactions. At these same pH values, we also see PA2 with the next highest CAC, leaving PA3 with the lowest CAC. This shows that the deletion of a single methylene group, with respects to PA1, has the smallest effect on the molecules ability to form micelles, if we assume that PA1 has a CAC of nearly zero for all pH values. This tells us that PA3 has the strongest tendency to form micelles as compared to PA2 and PA4.

We do see some discrepancy with the data at higher pH values in which the CAC trends previously described do not align. At a pH of 9, PA3 now has the highest CAC, followed by PA2 and finally PA4. It has been previously shown that at higher pH values the CAC levels off, and the degree of difference from one pH value to another is significantly less than in a more acidic environment. We see this in PA4, as the CAC at pH 7 is 14.08 μM and 15.45 μM at pH 9, showing little difference as compared to its CAC at pH 7 and at pH 5 (difference of 7.28 μM). However, for PA2 and PA3, there is no visible leveling off when it comes to the CAC, as the CAC difference for both of these PAs between pH 8 and pH 9 is greater than 9 μM, showing a sharp rise rather than a leveling off. At higher pH values, the five glutamic acids in PA2 will most likely all be deprotonated, making it more difficult for the PA to self-assemble. Likewise in PA3, even with four deprotonated glutamic acids, the shortened length of the alkyl tail also plays an important role in the molecule's ability to self-assemble into a micelle. Also the possible deprotonation of the two tyrosine residues (pKa = 10.07) could have a large effect on the single molecule-to-micelle aggregation.

Full Phase Diagrams:

Figure 10 shows all of the CD and CAC data for the three molecules for which phase diagrams were constructed. From this, we can conclude that the data that is obtained from CD cannot be transferred to CAC data. Essentially, it can be stated just because one of our PAs prefers a nanofiber morphology compared to a micelle, does not necessarily mean that it also prefers a micelle to a single molecule. We see this especially with PA4, as it has a more basic pH of transition via CD, but also consistently has the highest CAC. If we go off of the CD and CAC data that was found for PA2 and PA3, it would be expected that PA4 should have the lowest

CAC because of the more basic sphere to nanofiber transitional pH. This is opposite from what we see from the data as PA4 has the highest CAC.

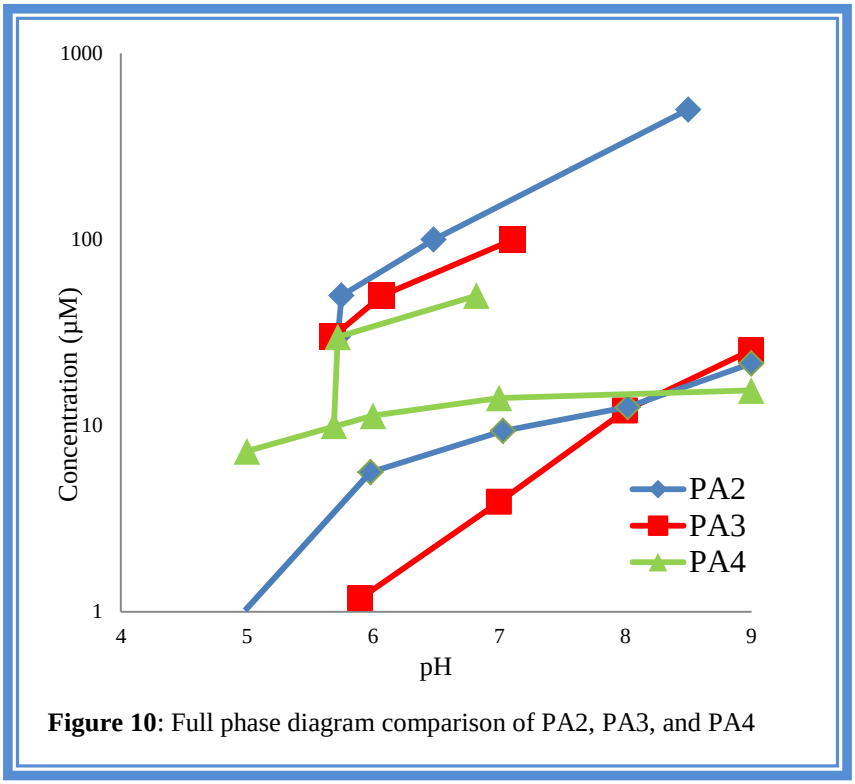

Figure 10: Full phase diagram comparison of PA2, PA3, and PA4

With PA2 and PA3, we do see that there is a more of an agreement data presented from CD and CAC. PA2 has a more acidic sphere to nanofiber transitional pH as well as a higher CAC as compared to PA3. This shows that PA2 has a lower affinity to self-assemble, either as a micelle or nanofiber, than PA3. Again this shows that the addition of a fifth glutamic acid to the molecule's charged region appears to have a greater effect on the molecule's ability to self-assemble rather than a deletion of methylene group from the alkyl tail.

Chapter 4: Conclusions and Future Work

In summary, we have been able to synthesize and characterize four different PAs to test how structural changes affect their self-assembly properties. CD and CAC have shown to be very effective methods for the construction of phase diagrams to these molecules. From these two methods, we have been able to show how the tested structural changes affect the morphological preferences of the PAs at differing concentrations and pH values. From the data, we see that all of these tyrosine based PAs show significant concentration dependent self-assembly properties than what we have previously seen. Increased the electrostatic forces as seen for PA2 shows a sphere to nanofiber transition at lower a pH than the deletion of a methylene group from the alkyl chain or the change of a tyrosine residue to an alanine, showing increased electrostatic repulsive forces makes it more difficult for the PA to self-assemble to a nanofiber than decreasing the attractive forces.

For the continuation of this project, more CD data for PA4 would need to be collected to test higher concentrations. These data points will lead to a more complete phase diagram of the molecule, thus leading to a better comparison to PA2 and PA3. Likewise, CD points for PA2 and PA3 at concentrations less than 30 μM will also lead to more complete data sets.

Chapter 5: Supporting Information

(i): Methods

Synthesis of Peptide Amphiphiles (PA):

All amino acids and coupling agents were purchased from AnaSpec INC. The peptides were synthesized via solid-phase Fmoc chemistry[19]. The peptide sequence was built C-Terminus to N-Terminus using a Seiber Amide Resin (AAPPTEC) on a 0.5 mmol scale. All of the prepared PAs were synthesized manually as outlined in the following paragraph.

The resin was placed in a shaker vessel and then swollen with dichloromethane (DCM) for 30 minutes. The DCM was removed, and then N, N-Dimethylformanide (DMF) was added to the shaker vessel to swell the resin for 30 minutes. Once the DMF was removed, 20% piperidine in DMF was added for the deprotection of the Fmoc protecting group and allowed to shake for 15 minutes. The liquid was removed, and replenished to shake for another 15 minute interval. The piperidine/DMF solution was removed and the resin was washed with DCM, DMF (2x) and DCM (2x) sequentially. The removal of the Fmoc protecting group was confirmed via a Kaiser Test. The coupling solution for each amino acid contained 4 eq. of O-Benzotriazole N,N,N',N'-tetramethyluroniumhexafluorophosphate (HBTU) or 2-(7-Aza-1H-benzotriazole-1-ly)-1,1,3,3- tetramethyluronium hexafluorophosphate (HATU), 3.95 eq. of amino acid, 6 eq. of N,N- diisopropylethylamine (DIPEA) and 3 drops of Triton X-100 in approximately 10 mL of DMF. This solution was added to the shaker vessel and allowed to couple for 3 hours to the deprotected species (amino acid or resin). The solution was then removed, and the resin was washed with DMF (3x) followed by DCM (2x). The coupling of the amino acid was confirmed

by another Kaiser Test. This process was repeated for each amino acid as well as the palmitic or pentadecanoic acid tail.

Resin Cleavage:

A 120 mL cleavage mixture was made containing 1% Trifluoroacetic acid (TFA), 2% Anisole and 97% DCM. The cleavage of the peptide from the resin was achieved by adding 20-25 mL portions of the cleavage mixture to the shaker vessel, and allowing it to shake for 25 minutes. After the allotted time, the solution was drained to a round-bottom flask, and another portion of the cleavage mixture was added to shake. Once all of the cleavage mixture was used, the TFA/DCM solution in the round-bottom flask was then neutralized with DIPEA. The excess solvent was removed under vacuum and the PA was precipitated out with cold water and cooled at 10 °C for 45-60 minutes. The resulting solid was then isolated via vacuum filtration.

Attachment of DO3A to PAs:

The solid PA was placed in a round bottom flask, along with 25 mL of pyridine. The mixture was shaken, sonicated, and then stirred in an oil bath at 60 °C for 60 minutes to ensure full dissolution of the PA. A coupling solution containing 2 eq. HATU, 2 eq. 1,4,7-tris(carboxymethylaza)cyclododecane-10-azaacetylamide (DO3A), 4.4 eq. DIPEA and a small portion (2-4 mL) of pyridine were added to the PA. All equivalents were with respect to the PA. The mixture was then set to stir for 18-24 hours at room temperature. To ensure maximal coupling, excess solvent was removed under vacuum, until only 10-15 mL of the mixture remained. A second coupling mixture of 2 eq. HATU, 4.4 eq. DIPEA and 1 mL of pyridine was added to the PA and stirred for 18-24 hours. The PA-DO3A was then crashed out with cold water and cooled at 10 °C for 45-60 minutes. The resulting PA-DO3A solid was isolated via vacuum filtration.

Removal of tert-butyl groups on PA:

A 20 mL solution containing 95% TFA, 3% water and 2% Anisole was prepared and added to the PA-DO3A. The mixture was set to stir for 20-24 hours at room temperature in order to remove tert-butyl groups from the glutamic acid, tyrosine and DO3A species. Excess TFA was removed under vacuum and the PA-DO3A was crashed out with cold diethyl ether. The mixture was cooled at -5°C for 45 minutes and the resulting solid was isolated via vacuum filtration.

Purification of PA-DO3A:

The crude PA-DO3A (150-250 mg) was dissolved in a 10 mL solution consisting of 9 mL of water, 1 mL of acetonitrile and a few drops of NH_4OH. This solution was shaken, sonicated and vortexed to ensure full dissociation. The resulting solution was then filtered through a 0.45 μm PVDF filter. Purification of the PA-DO3A was carried out using a Shimadzu preparative High Performance Liquid Chromatograph (HPLC) duel pump system controlled by LC-MS solution software, with an Agilent PLRP-S polymer column (Model No. PL1212.3100 150 mm x 25 mm). The two solvents that were used for the mobile phase were water with 0.1% NH_4OH (v/v) and acetonitrile with 0.1%NH_4OH (v/v). The product was eluted via a linear gradient from 10% acetonitrile to 20% acetonitrile over 22.5 minutes, and then from 20% acetonitrile to 40% acetonitrile over an additional 67.5 minutes. The desired product was collected in fractions of 10-15 mL. The presence of the product in the fractions was confirmed by a Bruker Electrospray Ionization Time of Flight Mass Spectrometry (ESI-TOF MS) and the fractions' purity was analyzed by a Shimadzu analytical HPLC. Fractions ≥ 95% in purity were added together, acetonitrile was removed under vacuum and the liquid fraction were freeze-dried yield a white powder.

Incorporation of Gd^{3+} in PA-DO3A:

The pure PA-DO3A was dissolved in 4-6 mL of water. 2 eq. of 0.01M $GdCl_3$ in 0.01M HCl were added to the PA-DO3A solution. Diluted NaOH(aq) was added to this solution to set the pH at 5.0 - 5.1. The solution was placed in an oil bath to stir at 60°C. After 60 minutes, the solution was removed from the oil bath, the pH was readjusted to a value of 5.0 – 5.1, and placed back in the hot oil bath to stir for 12-18 hours. The solution was then returned to room temperature and the pH was raised to a value greater than 10 using 1 M NaOH to precipitate out all non-chelated Gd^{3+} to produce solid $Gd(OH)_3$. The solution was filtered with a 0.45 µm PVDF filter and the pH was lowered to a neutral value of approximately 7.

Dialysis of the PA-(DO3A:Gd):

The PA-(DO3A:Gd) solution was pipetted into a Spectra/Por® Biotech Cellulose Ester dialysis membrane (molecular weight cut off: 500 g/mol) and placed in 4 L of Millipore water. The water was changed 10-12 times over a 72 hour period. The dialyzed solution was then freeze-dried. The resulting solid yielded the pure PA-(DO3A:Gd) powder which was confirmed through ESI- TOF MS and analytical HPLC.

Circular Dichorism (CD):

The PA-(DO3A:Gd) solid was dissolved in a aqueous solution of 150 mM NaCl and 2.2 mM $CaCl_2$, to yield a 0.5 – 1 mM peptide solution. The resulting solution was then used to create diluted samples that included 100, 50, 30 and 10 µM. The pH was raised in each of the solutions to a value greater than 9, stirred in an oil bath at 90 °C for 30 minutes, and then cooled to room temperature. CD measurements were conducted on a JASCO J-815 Spectrometer using a 0.5 or 1 cm path length quartz cuvette. Three accumulation were measured at a wavelength

range of 260 – 190 nm at a scanning speed of 100 nm/min with an integration time of 2 or 4 seconds for each data series. A baseline (aqueous salt solution) was subtracted from each of the measurements. Each molecule in this study was analyzed with these parameters at different concentration and pH values.

Critical Aggregation Concentration (CAC):

CAC for the synthesized molecules were determined using the pyrene 1:3 method[23]. CAC measurements were taken at pH points of 5, 6, 7, 8, and 9 for each of the molecules tested. 5 mg of pyrene were dissolved and mixed in methanol overnight and then diluted with NaCl, $CaCl_2$ aqueous solutions, and excess water to yield a solution of 150 mM NaCl, 2.2 mM $CaCl_2$ and 62 µM pyrene.

For the 500 µM PA-(DO3A:Gd) solution, the pH was raised to a value greater than 9, stirred in an oil bath at 90 °C for 30 minutes, and then cooled to room temperature. A 300 µM sample was made from this solution. 250 µL of both the 500 µM and 300 µM solutions were serial diluted with 150 mM NaCl 2.2 $CaCl_2$ mM aqueous solution. Each of the starting concentrations and the diluted mixtures were added to a 96-microwell plate. 5 µL of the pyrene solution was added to each of the wells and then stirred to ensure homogeneity. All of the components added to make the samples were at the same pH value in order to test the CAC. The fluorescence emission of the pyrene was monitored by a BioTek Synergy H4 fluorimeter at an excitation wavelength of 335 nm. The pyrene fluorescence was monitored from 360 nm to 430 nm, and the peaks of maximum fluorescence intensity (usually at 376 nm and 392 nm) were compared at different concentration values to determine the CAC at a specific pH value.

Transmission Electron Microscopy (TEM):

The PA-(DO3A:Gd) sample (typically 100-500 µM) was raised to a pH value greater than 9, stirred in an oil bath at 90 °C for 30 minutes, and then cooled to room temperature. The pH was then adjusted to desired value using HCl and/or NaOH aqueous solution. Once the pH was reached, 5 µL of the sample was placed and spread onto a Carbon Formvar grid (Electron Microscopy Sciences) and allowed to sit for 45 seconds before being wicked dry. A 1 wt% uranyl acetate solution was added and spread over the grid to negatively stain the sample, and was wicked dry immediately after application. The grid was then examined by a FEI Tecnai G2 Biotwin TEM.

(ii): Final Product Analysis

Figure S1: Analytical HPLC of pure PA-(DO3A: Gd) Samples.

palmitoyl-YYAAEEEEK(DO3A:Gd)-NH_2 (PA1)

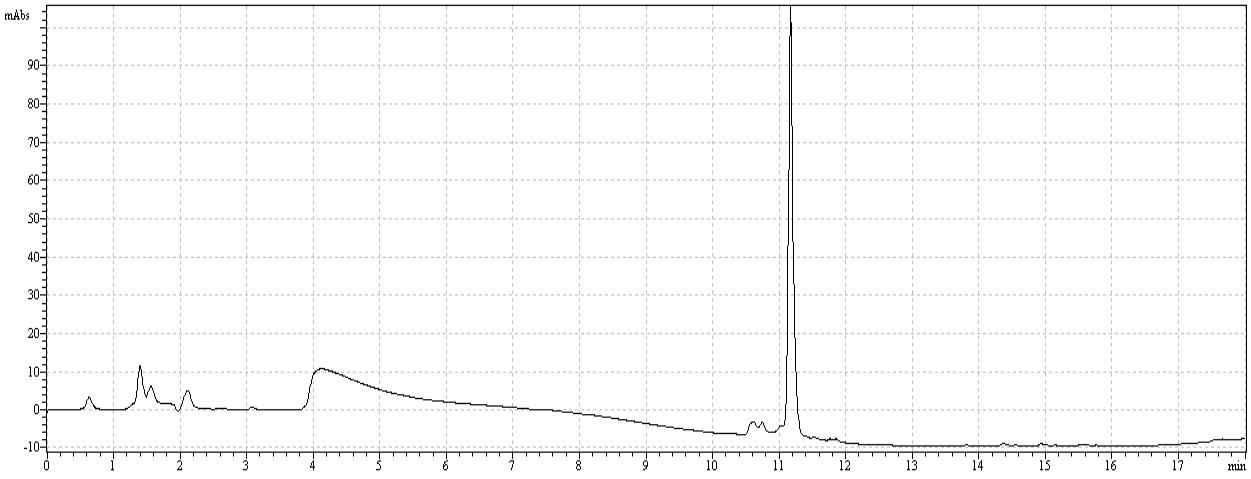

palmitoyl-YYAAEEEEEK(DO3A:Gd)-NH_2 (PA2)

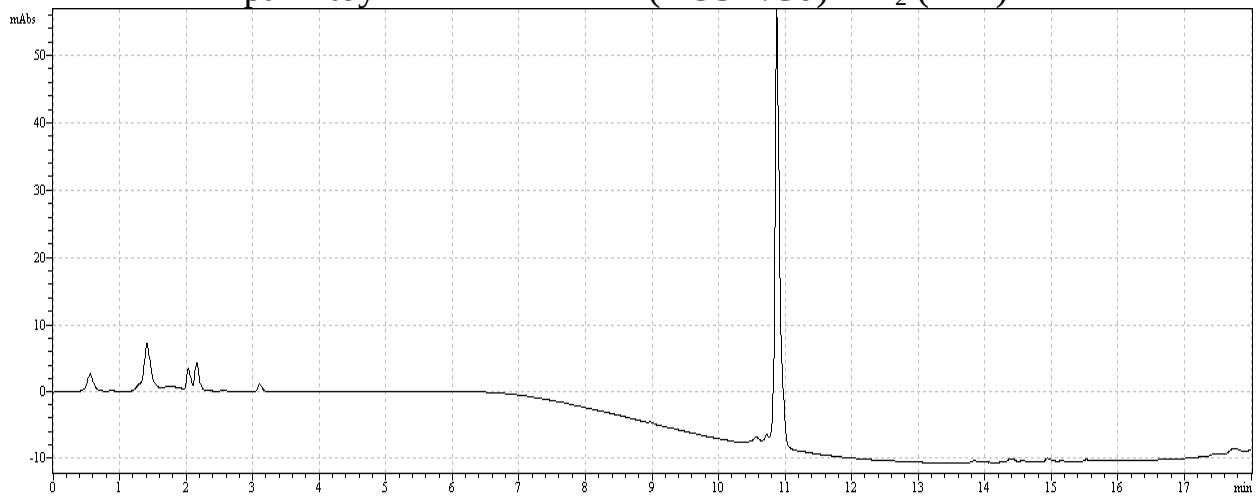

pentadecyl-YYAAEEEEK(DO3A:Gd)-NH_2 (PA3)

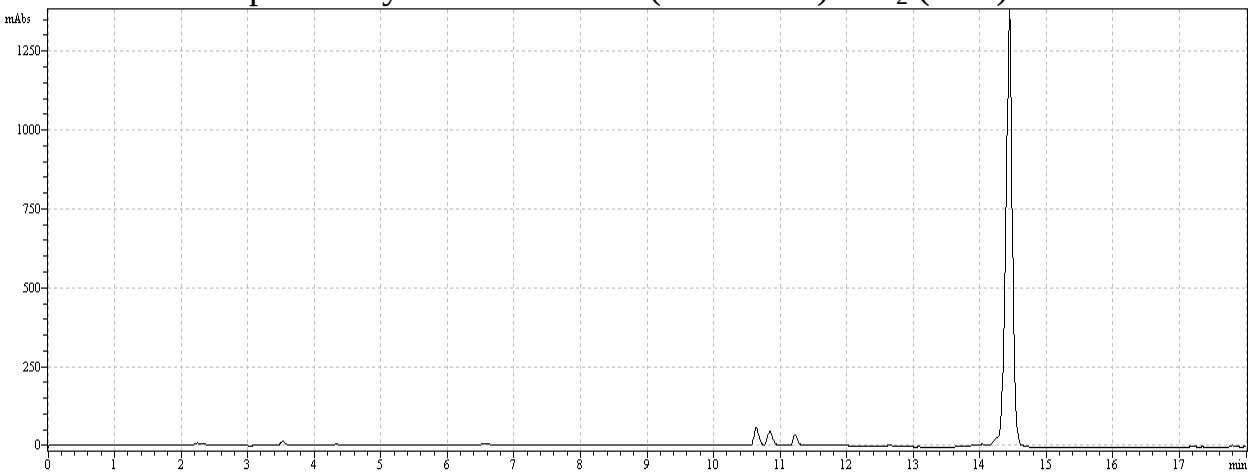

palmitoyl-YAAAEEEEEK(DO3A:Gd)-NH_2 (PA4)

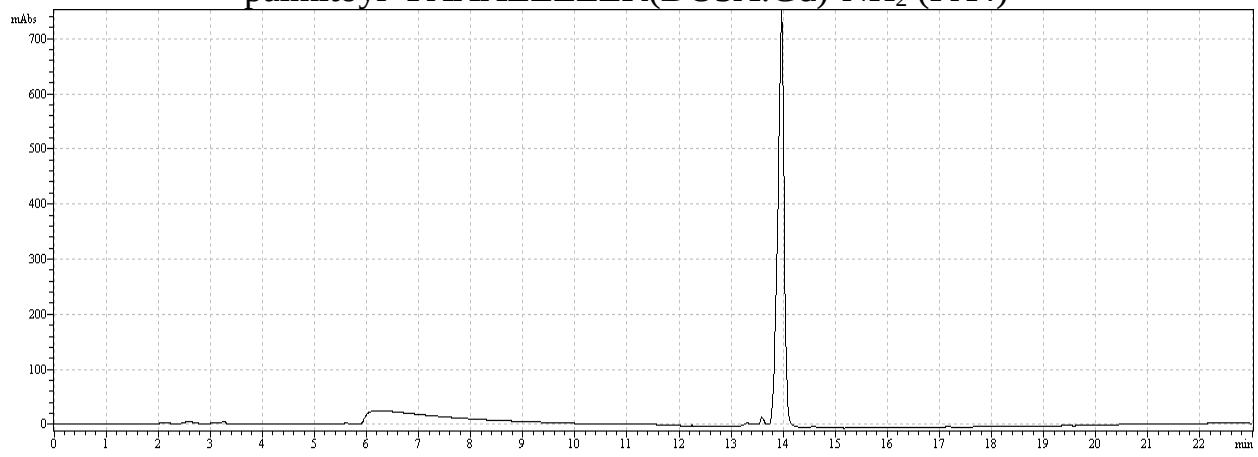

Figure S2: ESI- TOF MS (All in Positive Mode).

palmitoyl-YYAAEEEEK(DO3A:Gd)-NH_2 (MW: 1909.22g/mol)

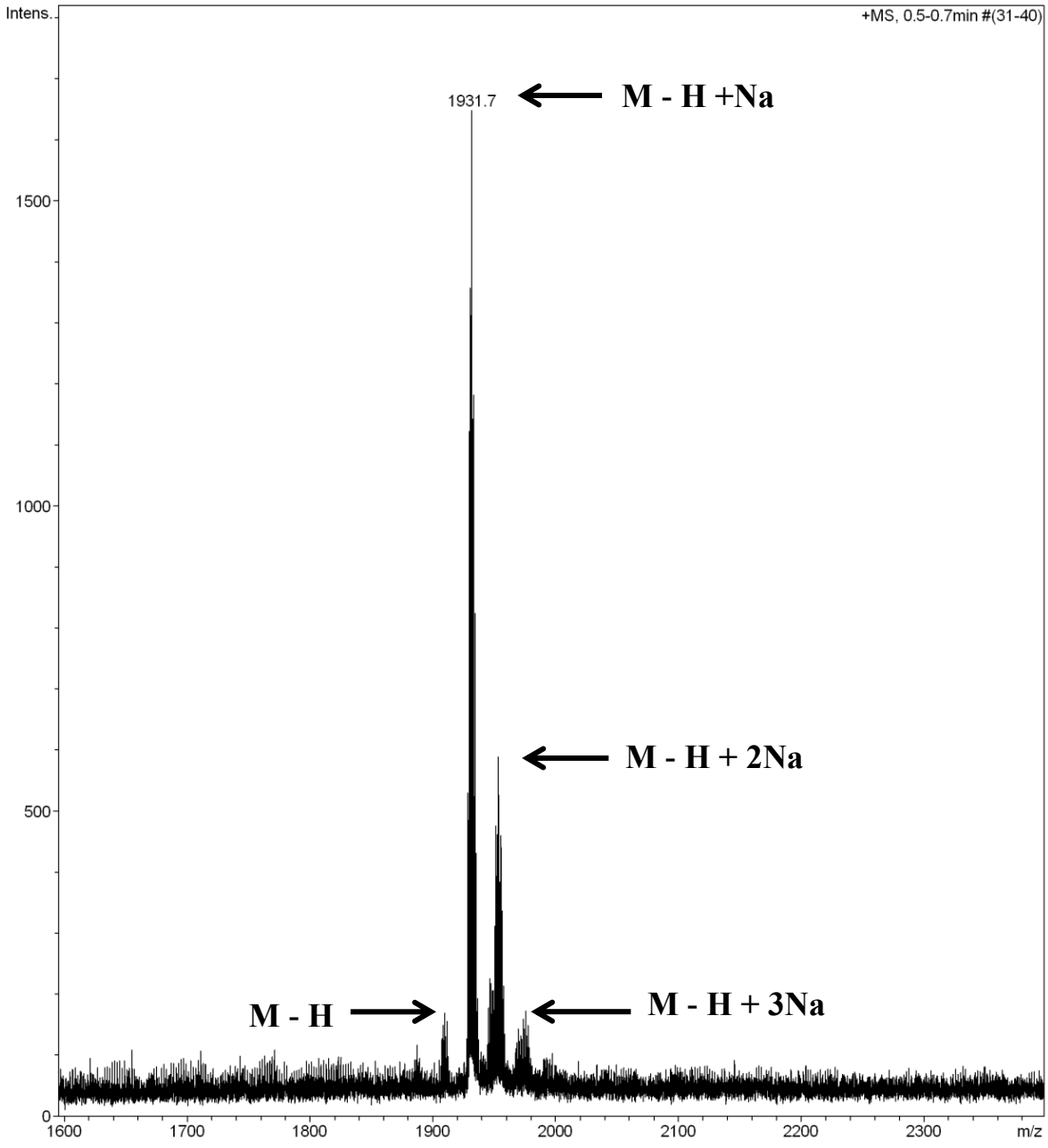

palmitoyl-YYAAEEEEEK(DO3A:Gd)-NH_2 (MW: 2038.34 g/mol)

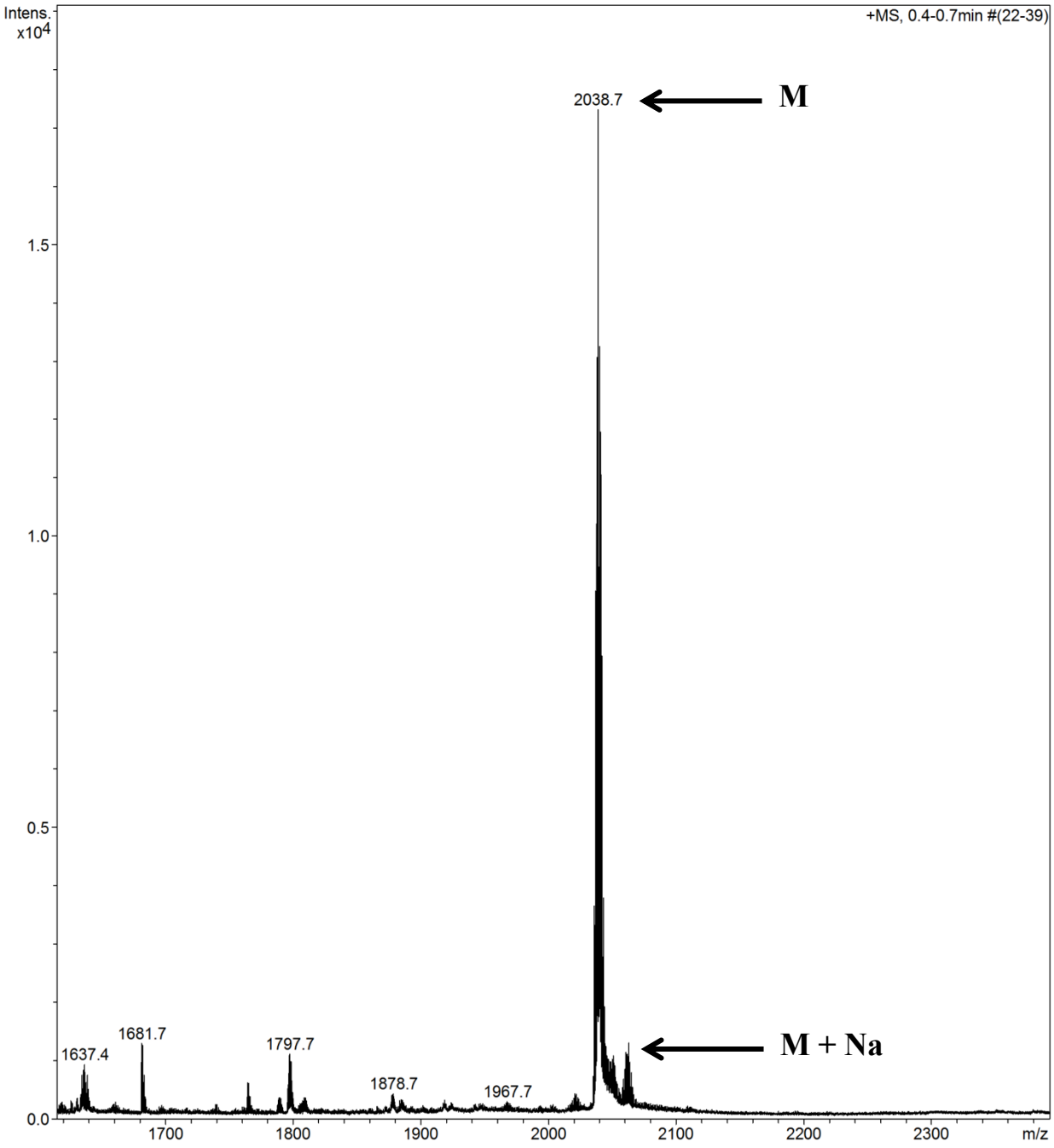

pentadecyl-YYAAEEEEK(DO3A:Gd)-NH_2 (MW: 1895.20 g/mol)

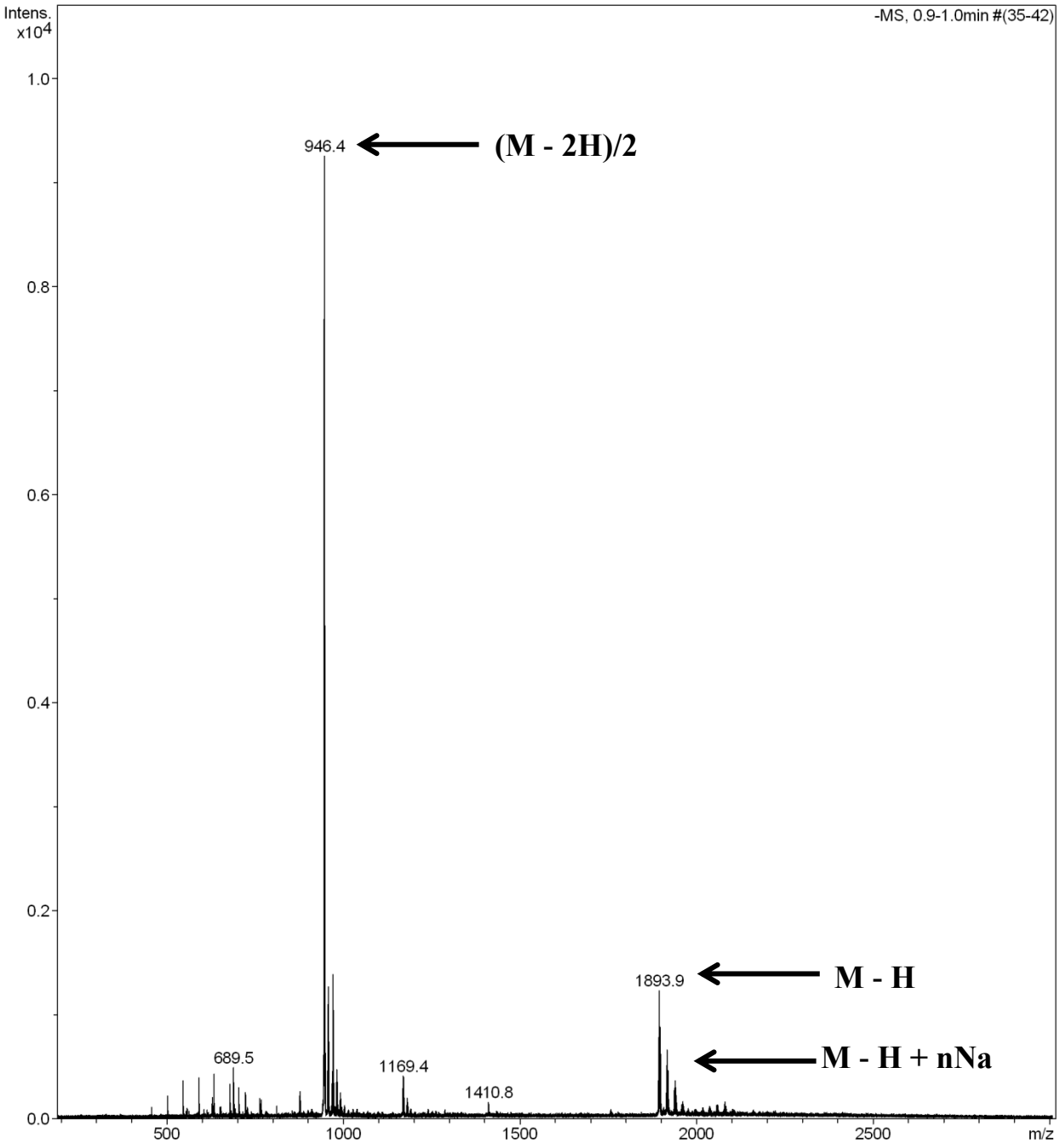

palmitoyl-YAAAEEEEEK(DO3A:Gd)-NH_2 (MW: 1818.11 g/mol)

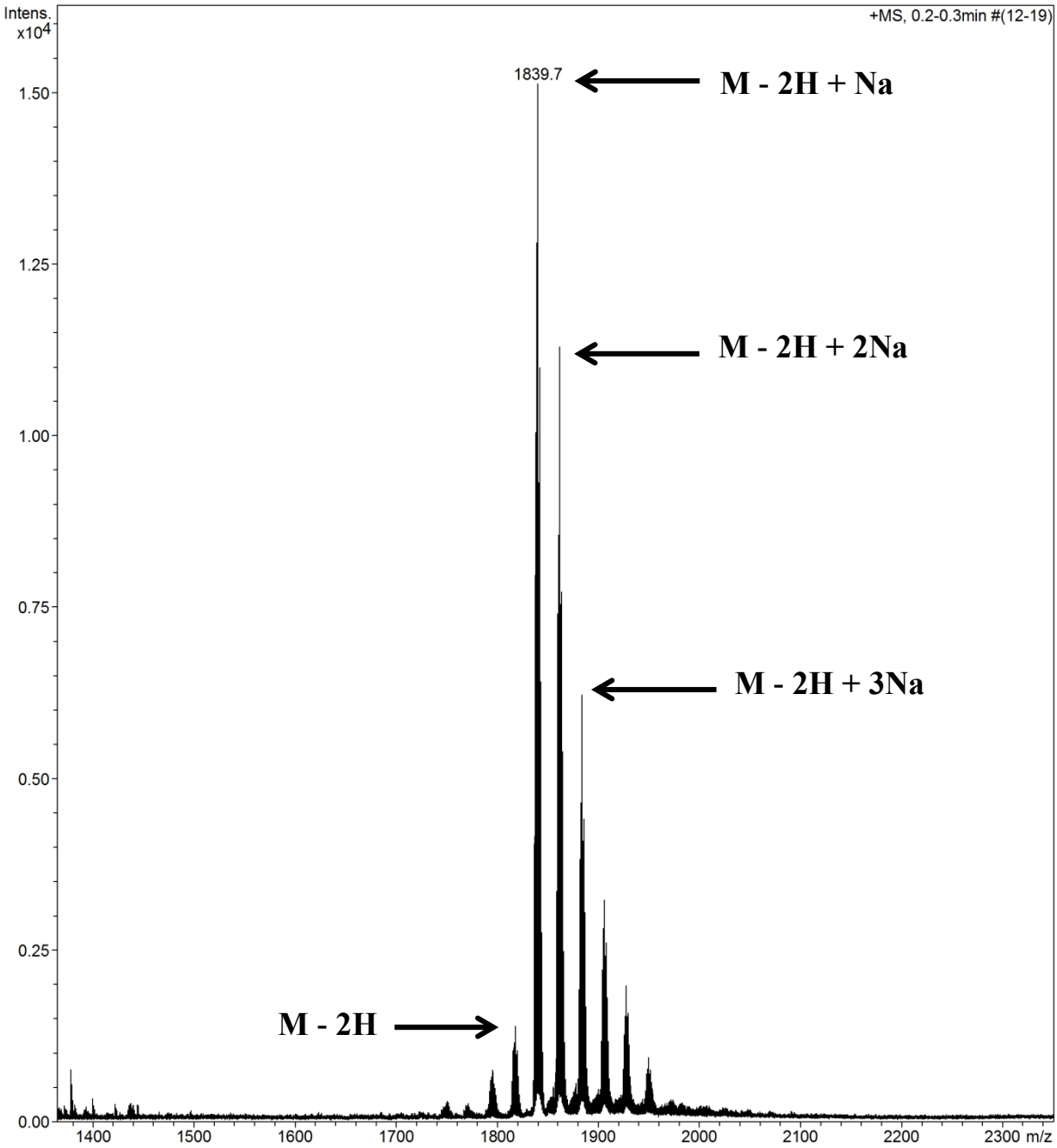

Figure S3: Circular Dichorism Data:

- PA1 at 500 µM in 150 mM NaCl and 2.2 mM $CaCl_2$.

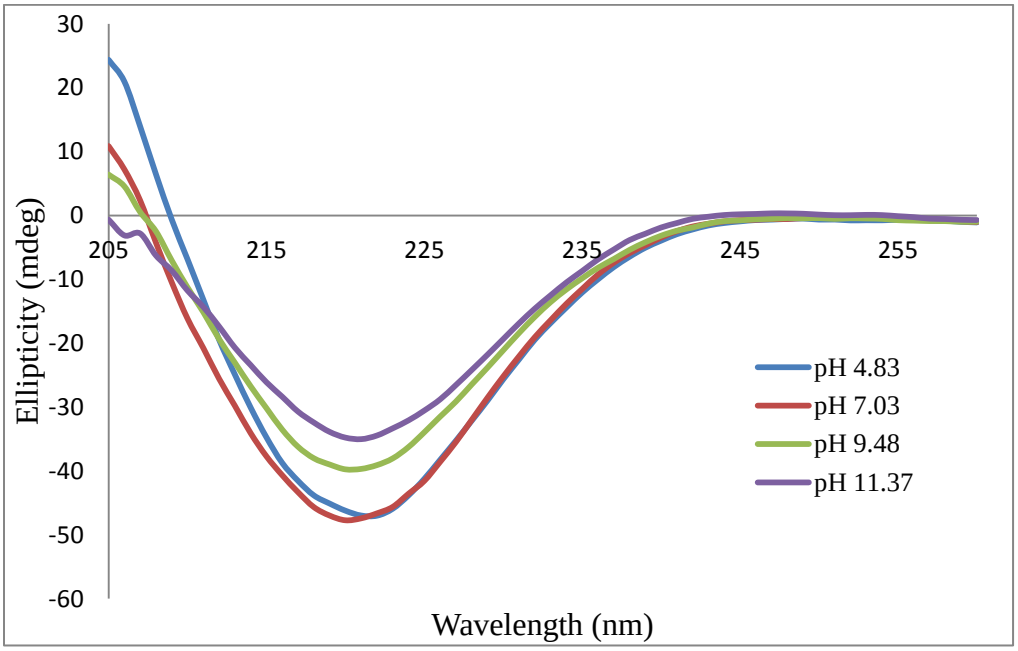

- PA2 at different concentrations in 150 mM NaCl and 2.2 mM $CaCl_2$ for phase diagram.

500 µM

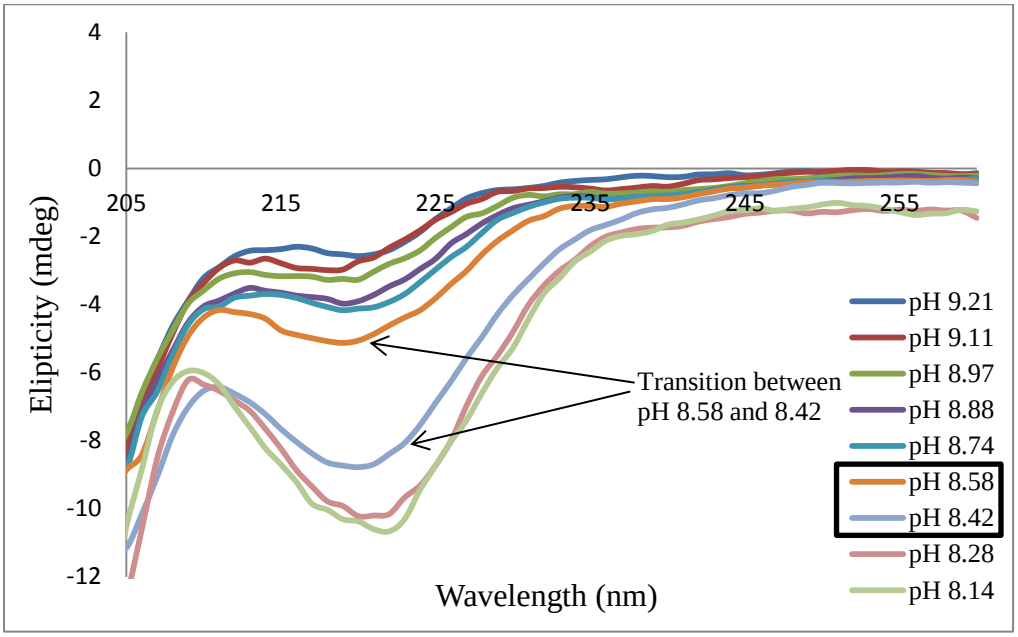

100 µM

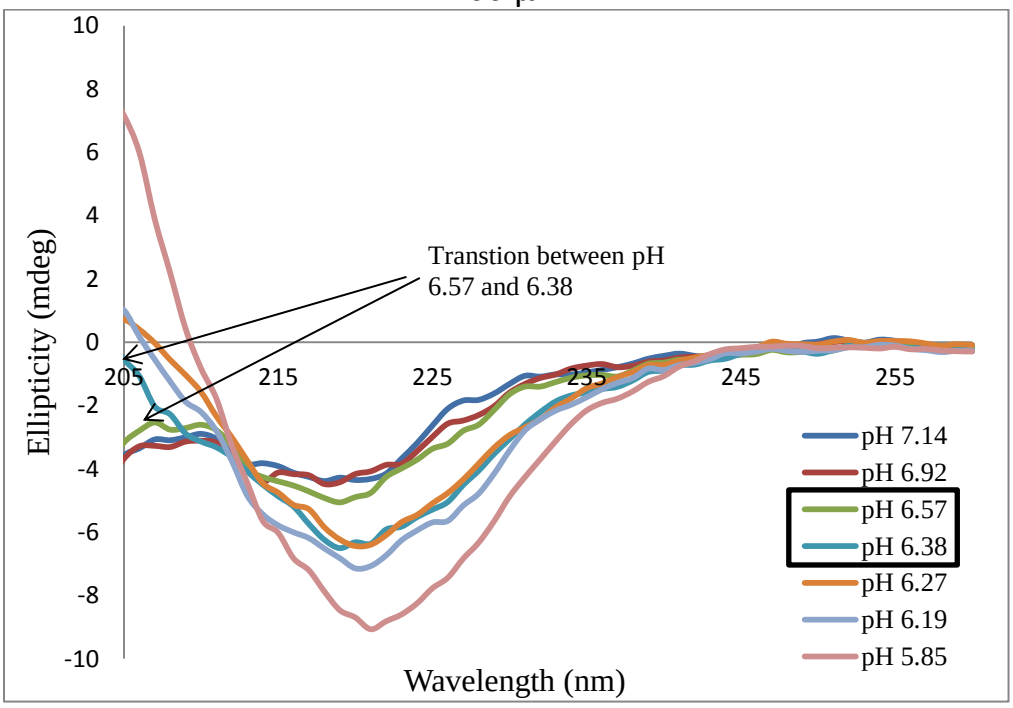
10
8
6
4
2
0
-2
-4
-6
-8
-10
205
215
225
235
245
255
Ellipticity (mdeg)
Wavelength (nm)
Transtion between pH 6.57 and 6.38
pH 7.14
pH 6.92
pH 6.57
pH 6.38
pH 6.27
pH 6.19
pH 5.85

30 µM

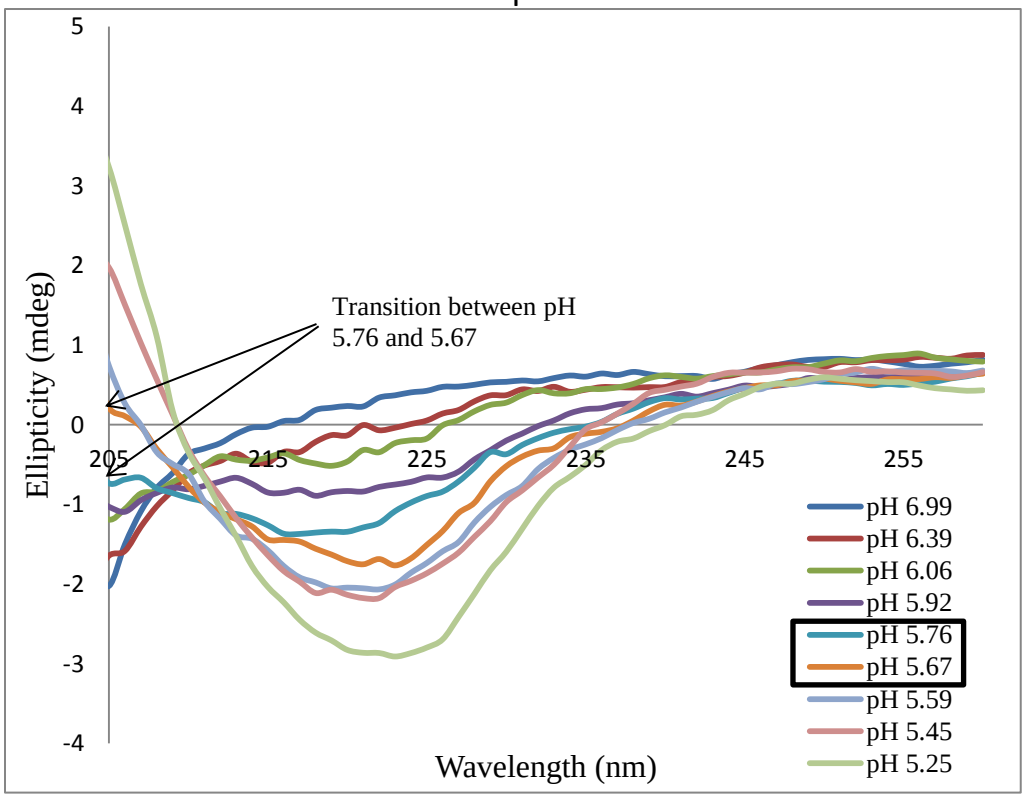
5
4
3
2
1
0
-1
-2
-3
-4
205
215
225
235
245
255
Ellipticity (mdeg)
Wavelength (nm)
Transition between pH 5.76 and 5.67
pH 6.99
pH 6.39
pH 6.06
pH 5.92
pH 5.76
pH 5.67
pH 5.59
pH 5.45
pH 5.25

- PA3 at different concentrations in 150 mM NaCl and 2.2 mM $CaCl_2$ for phase diagram.

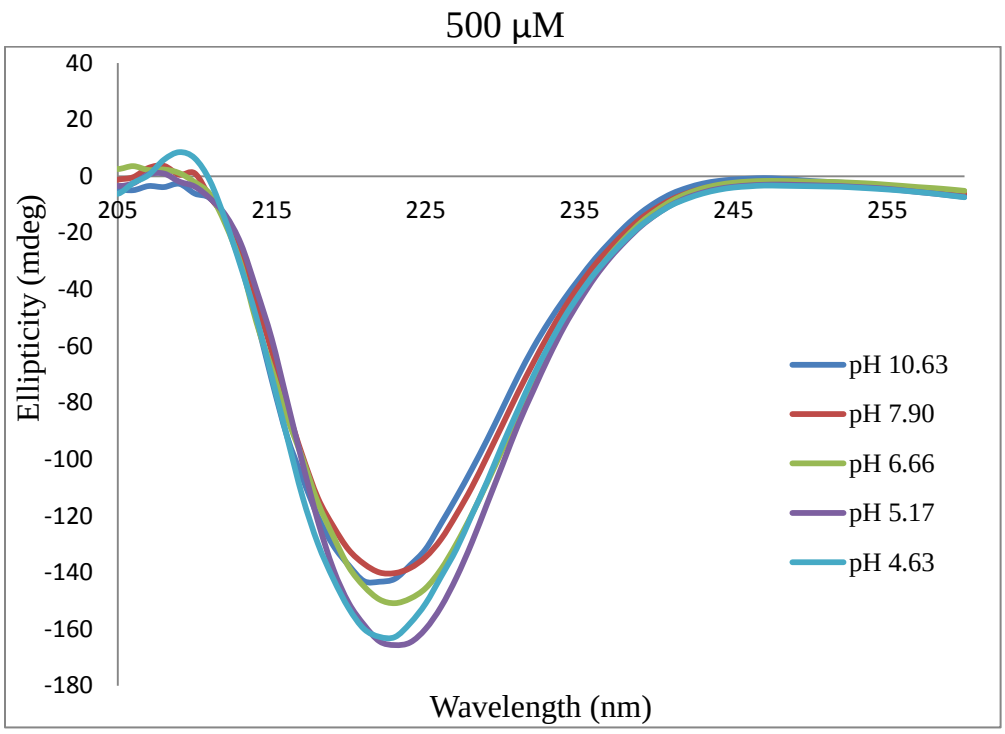

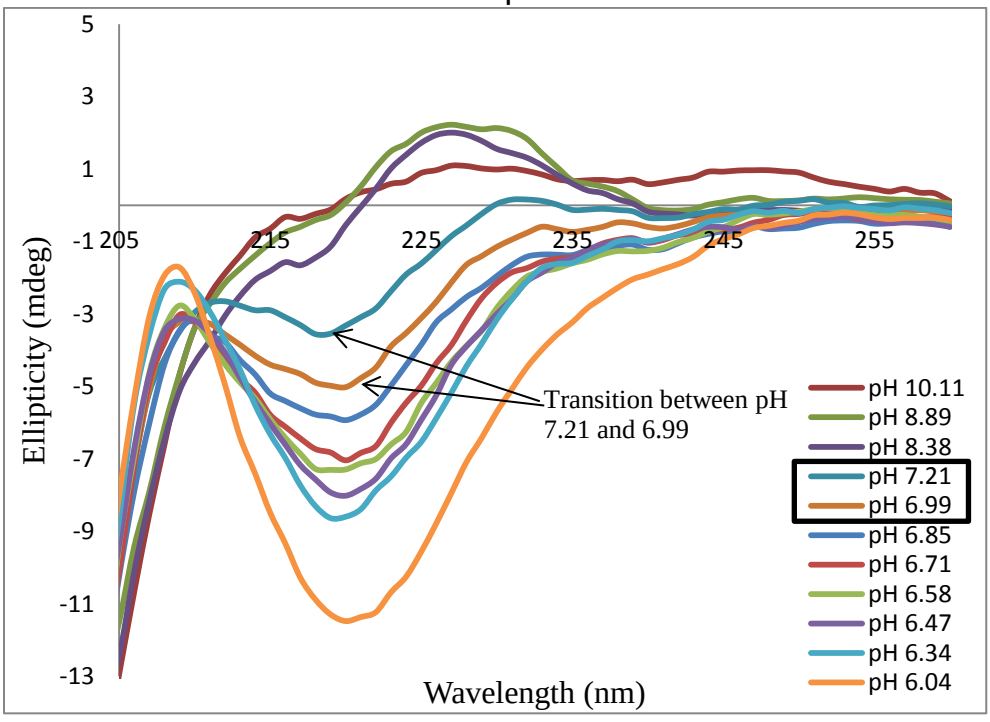

50 µM

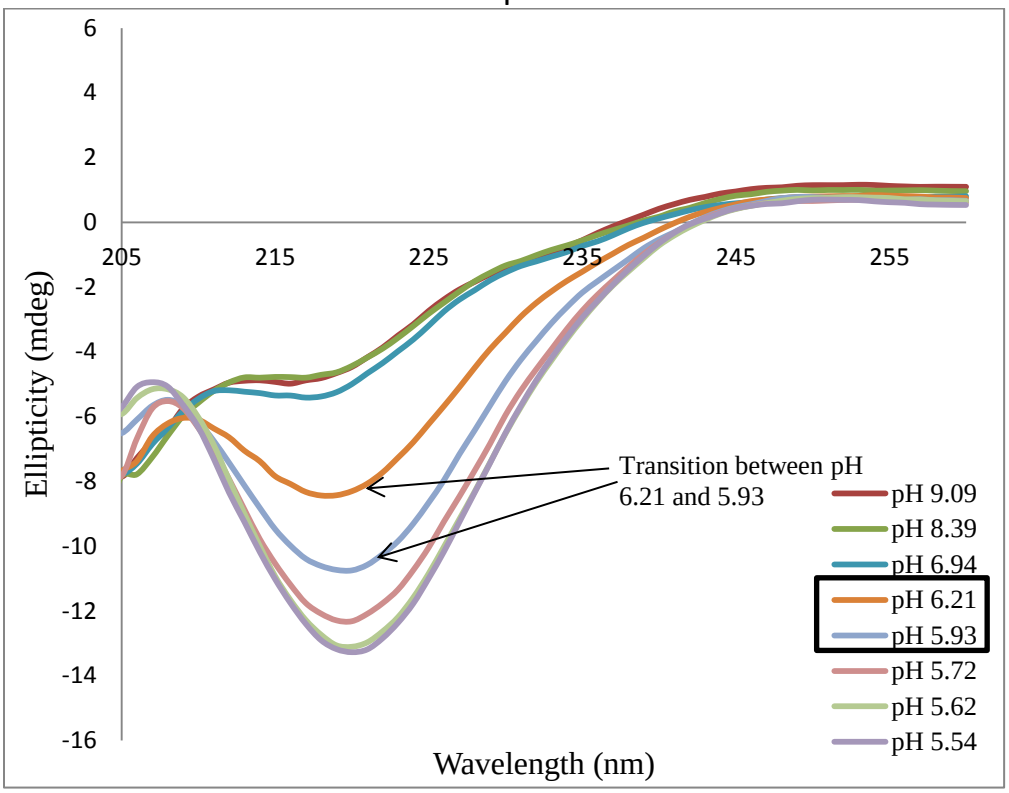
6
4
2
0
205
215
225
235
245
255
-2
-4
-6
-8
-10
-12
-14
-16
Ellipticity (mdeg)
Transition between pH
6.21 and 5.93
pH 9.09
pH 8.39
pH 6.94
pH 6.21
pH 5.93
pH 5.72
pH 5.62
pH 5.54
Wavelength (nm)

30 µM

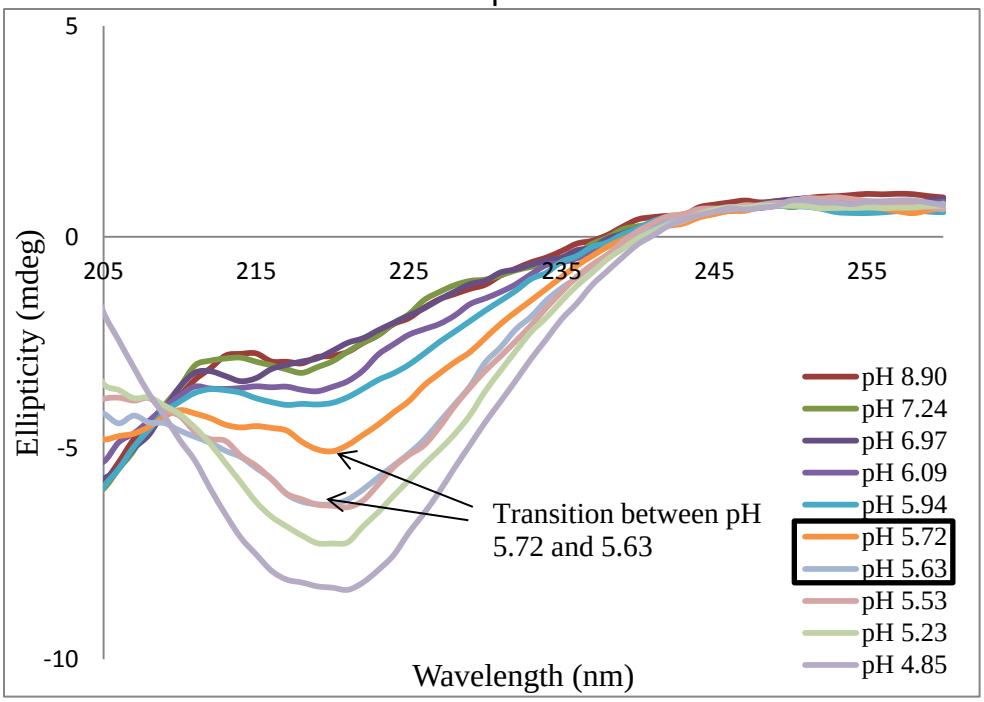
5
0
205
215
225
235
245
255
-5
-10
Ellipticity (mdeg)
Transition between pH
5.72 and 5.63
pH 8.90
pH 7.24
pH 6.97
pH 6.09
pH 5.94
pH 5.72
pH 5.63
pH 5.53
pH 5.23
pH 4.85
Wavelength (nm)

- PA4 at different concentrations in 150 mM NaCl and 2.2 mM $CaCl_2$ for phase diagram.

50 μM

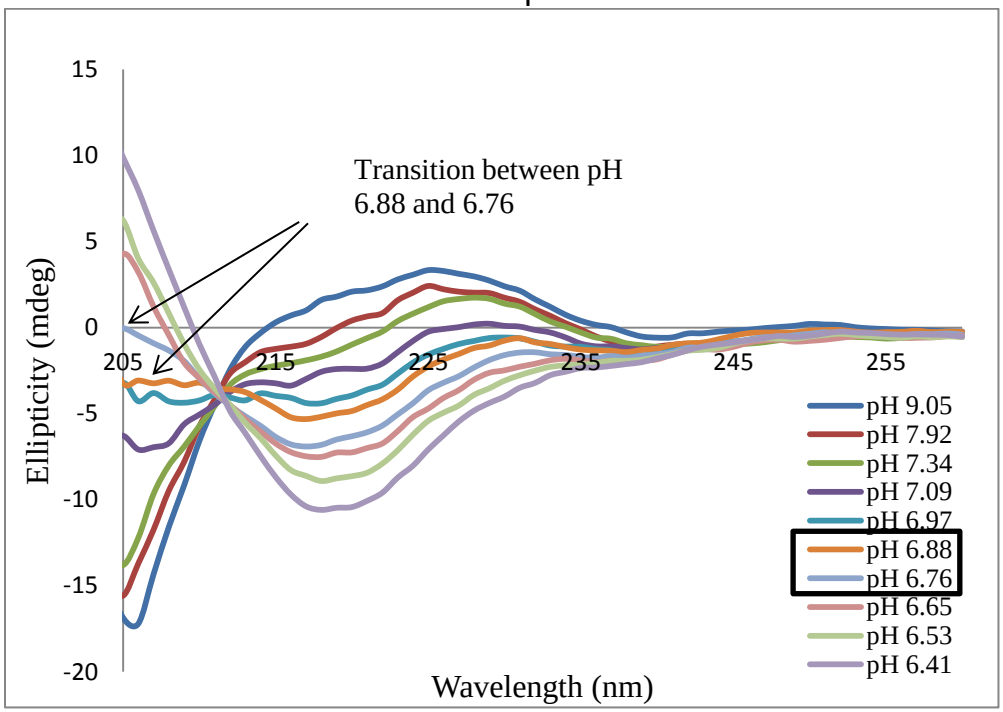

30 μM

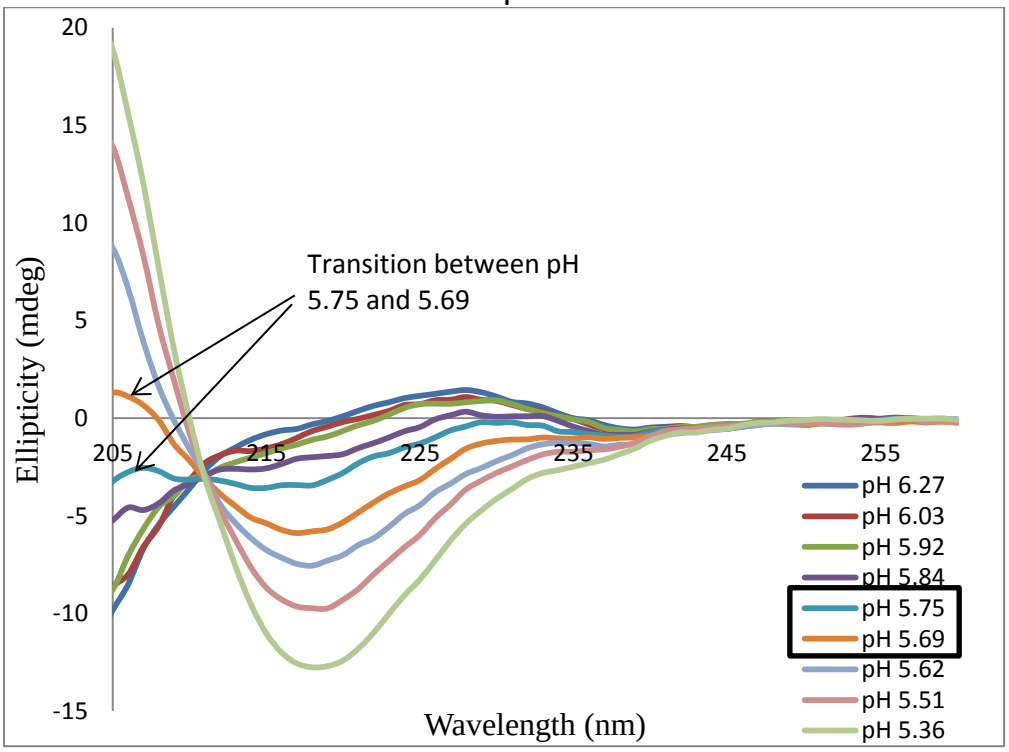

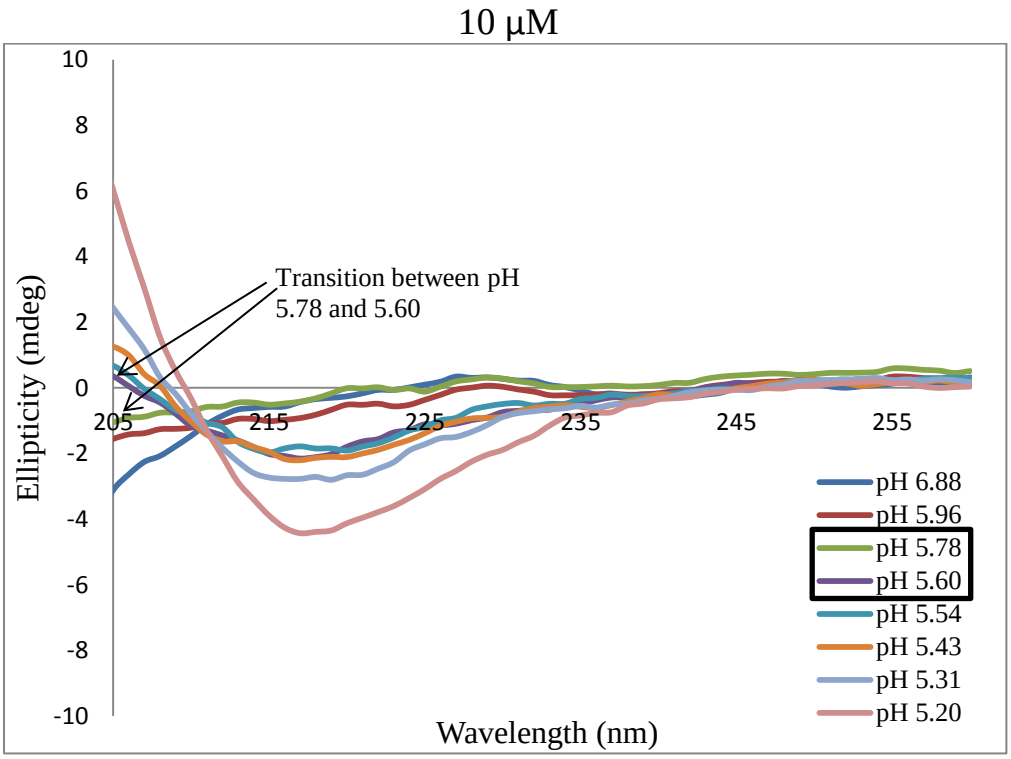

Figure S4: Critical Aggregation Concentration Data

- PA2 at pH values in 150 mM NaCl and 2.2 mM $CaCl_2$ for phase diagram.

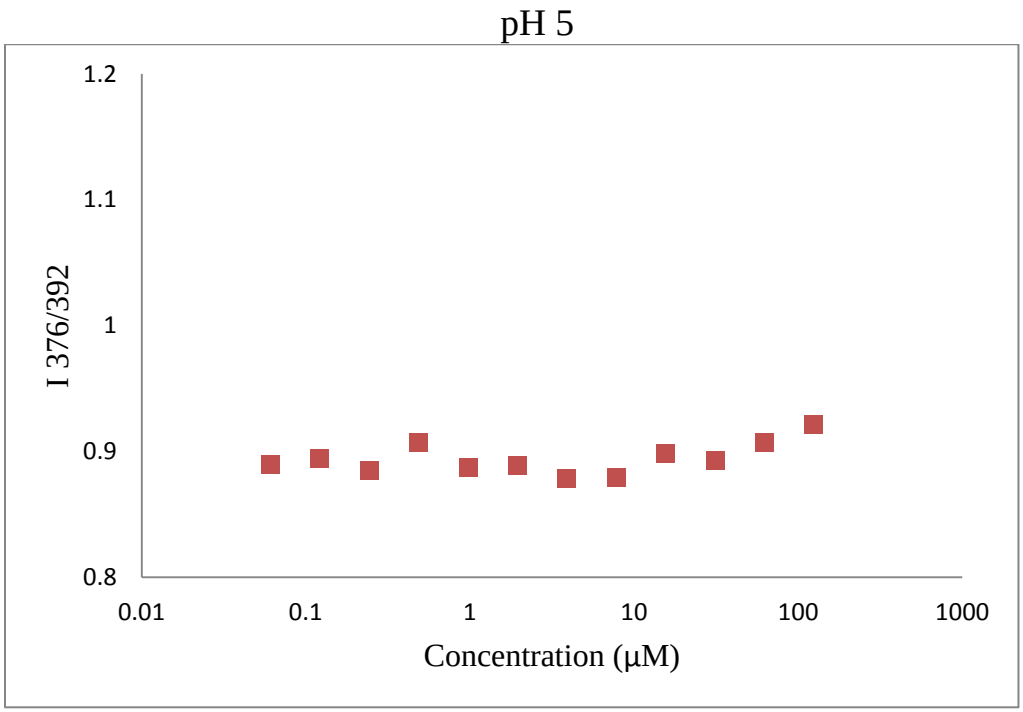

pH 6

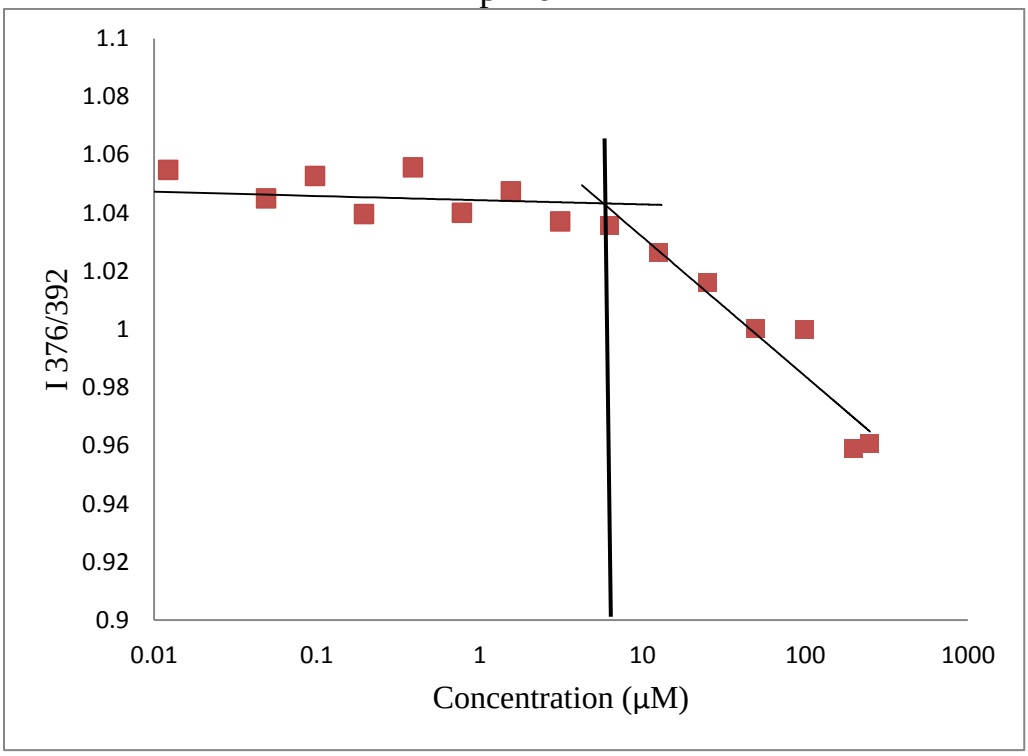
1.1
1.08
1.06
1.04
1.02
1
0.98
0.96
0.94
0.92
0.9
I 376/392
0.01
0.1
1
10
100
1000
Concentration (µM)

pH 7

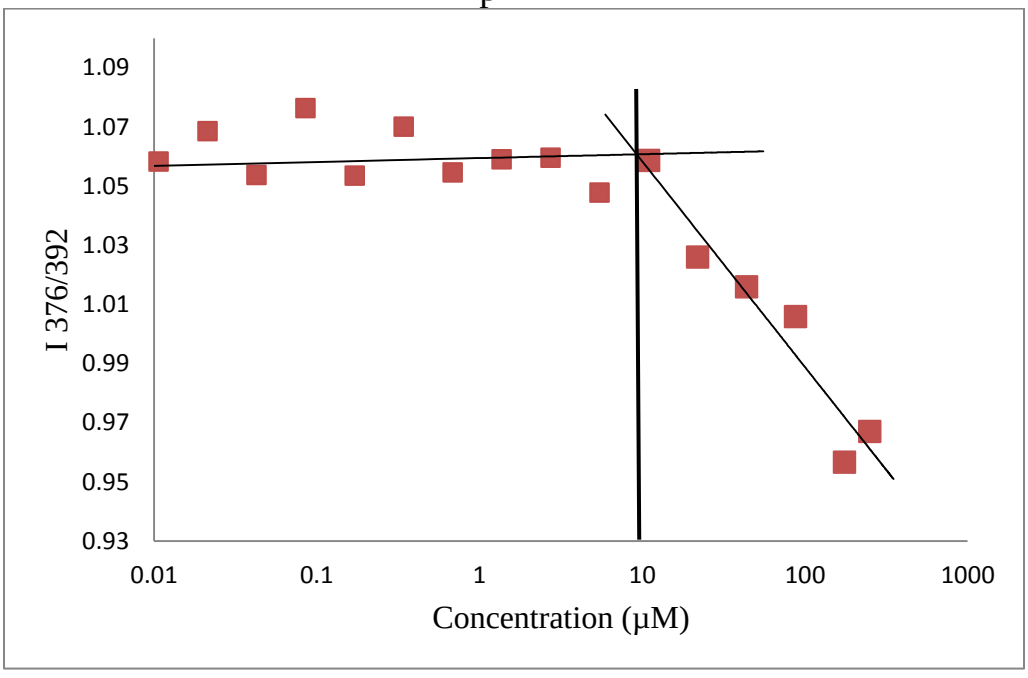
1.09
1.07
1.05
1.03
1.01
0.99
0.97
0.95
0.93
I 376/392
0.01
0.1
1
10
100
1000
Concentration (µM)

pH 8

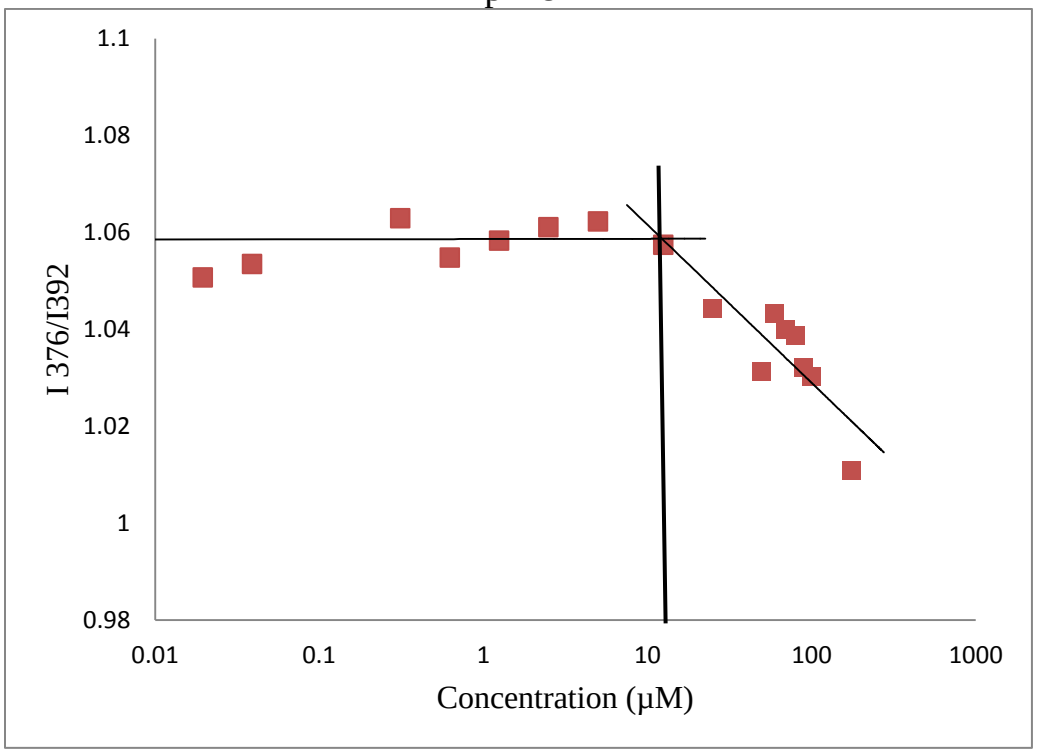
1.1
1.08
1.06
1.04
1.02
1
0.98
I 376/I392
0.01
0.1
1
10
100
1000
Concentration (µM)

pH 9

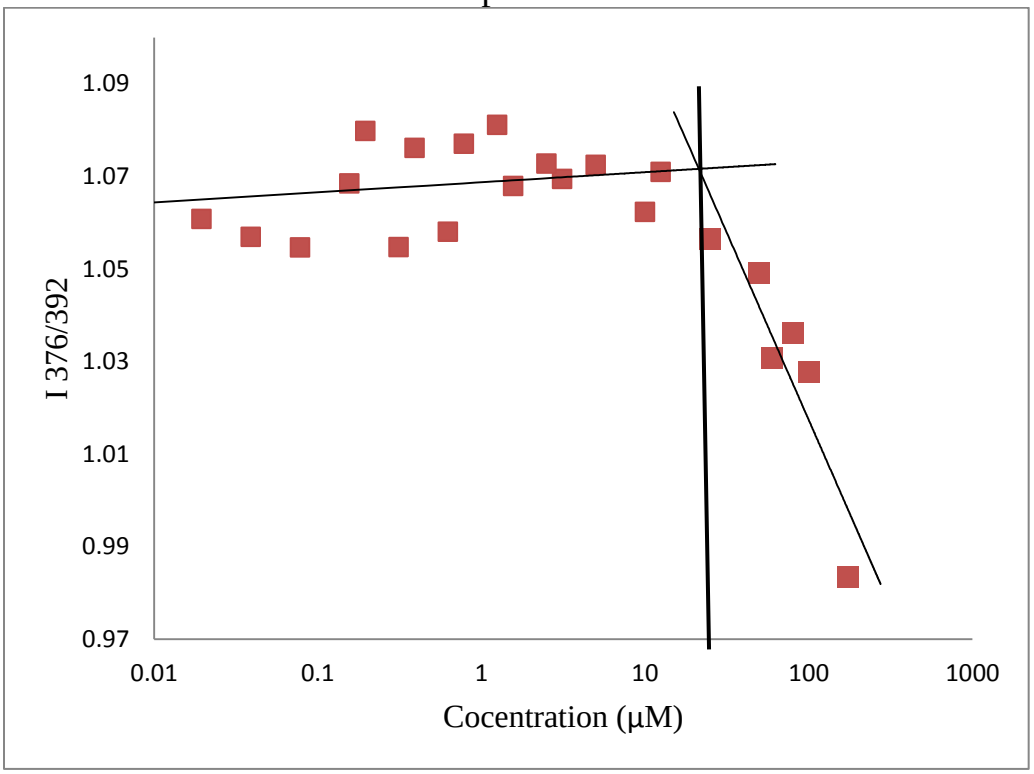
1.09
1.07
1.05
1.03
1.01
0.99
0.97
I 376/392
0.01
0.1
1
10
100
1000
Cocentration (µM)

- PA3 at pH values in 150 mM NaCl and 2.2 mM $CaCl_2$ for phase diagram

pH 6

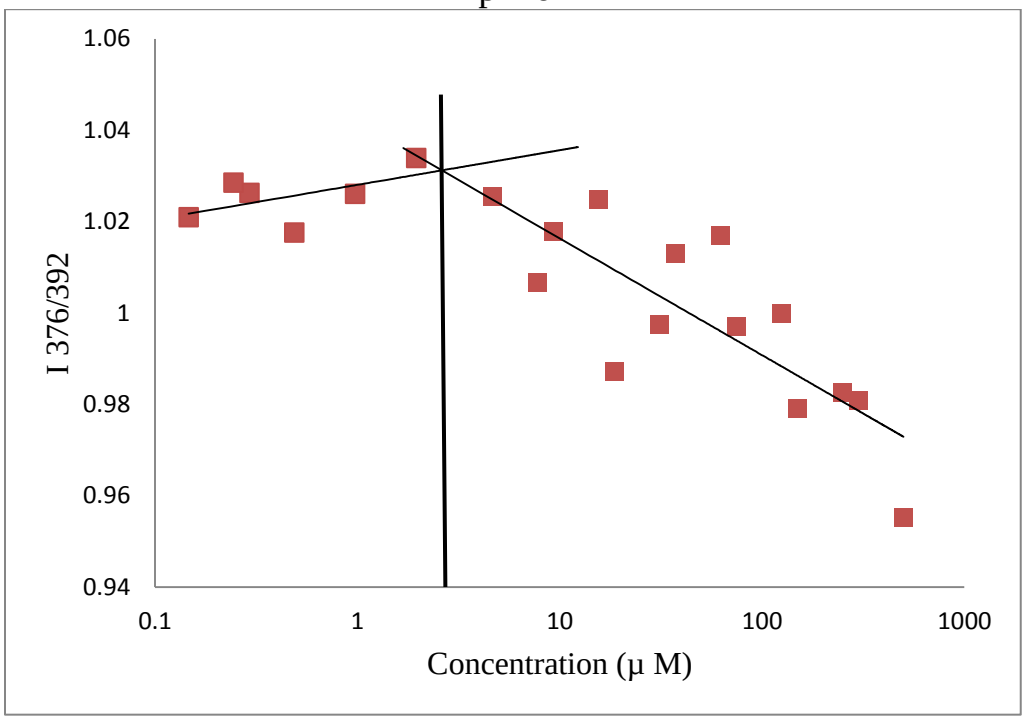

pH 7

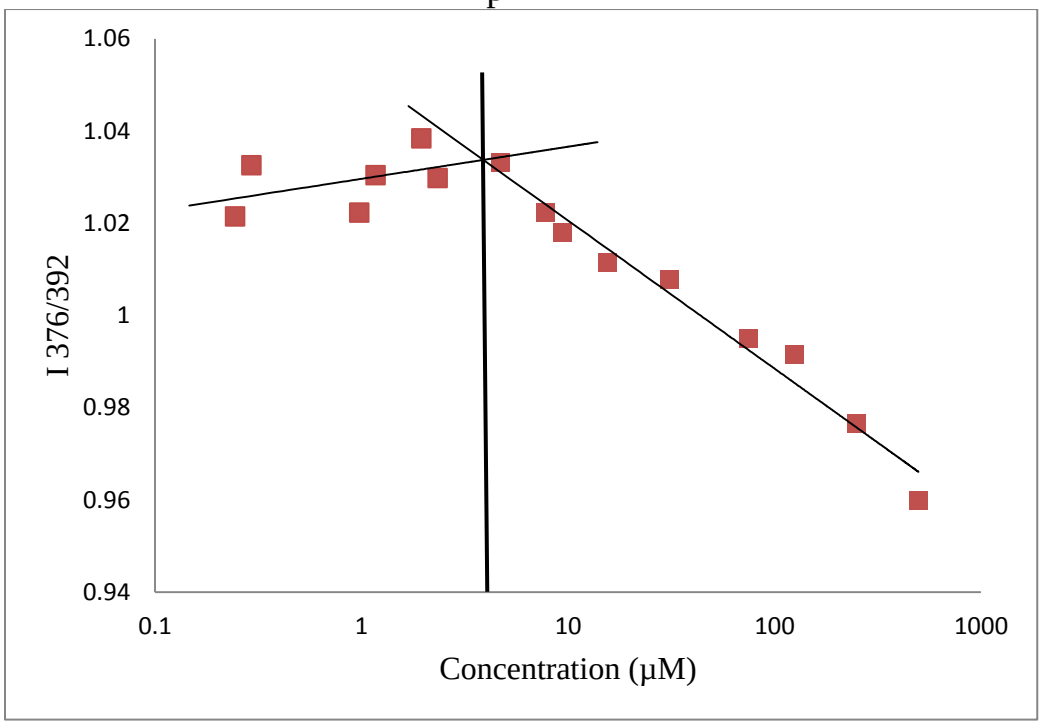

pH 8

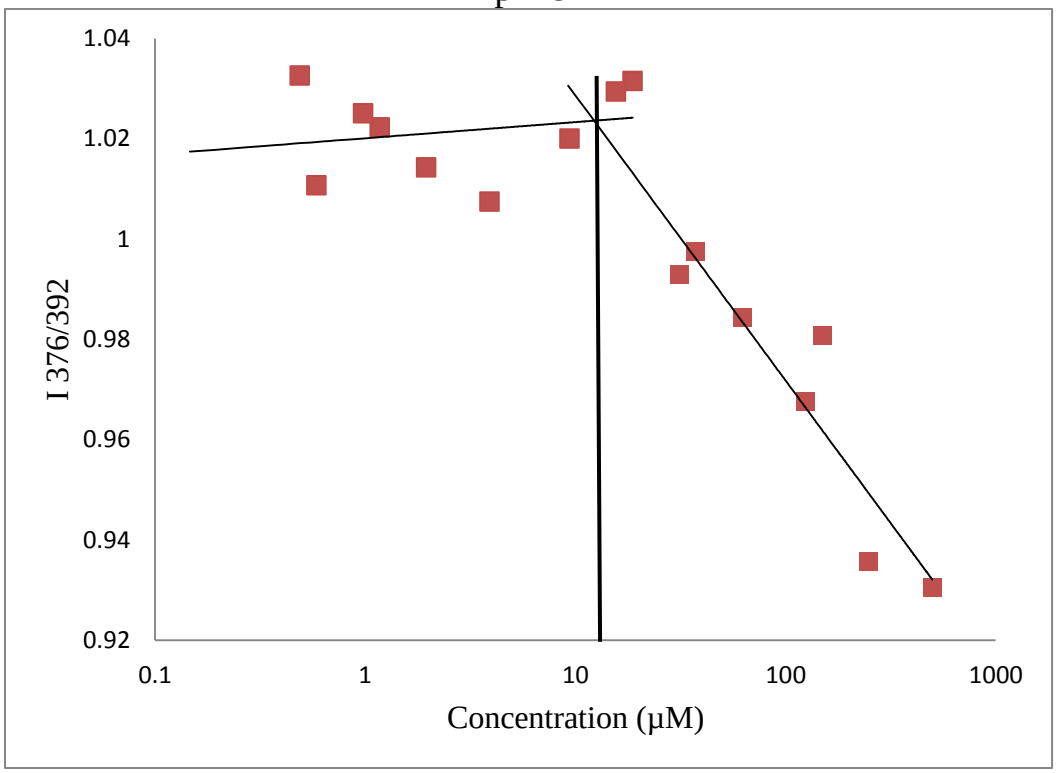
1.04
1.02
1
0.98
0.96
0.94
0.92
I 376/392
0.1
1
10
100
1000
Concentration (µM)

pH 9

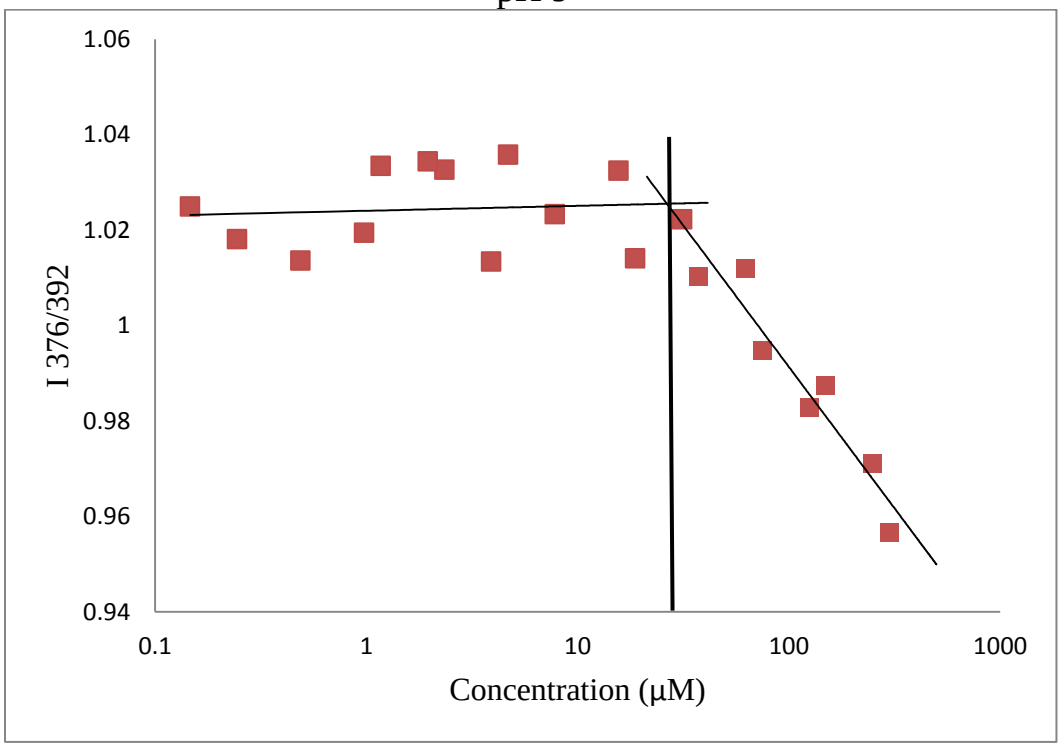
1.06
1.04
1.02
1
0.98
0.96
0.94
I 376/392
0.1
1
10
100
1000
Concentration (µM)

- PA4 at pH values in 150 mM NaCl and 2.2 mM $CaCl_2$ for phase diagram

pH 5

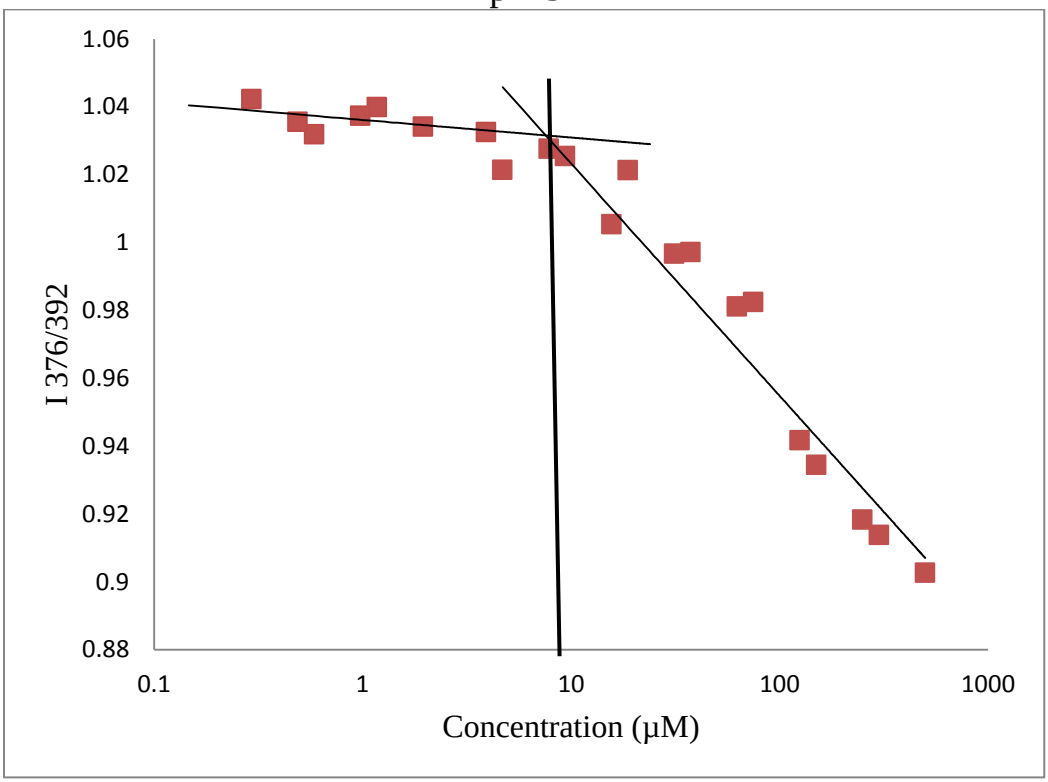

pH 6

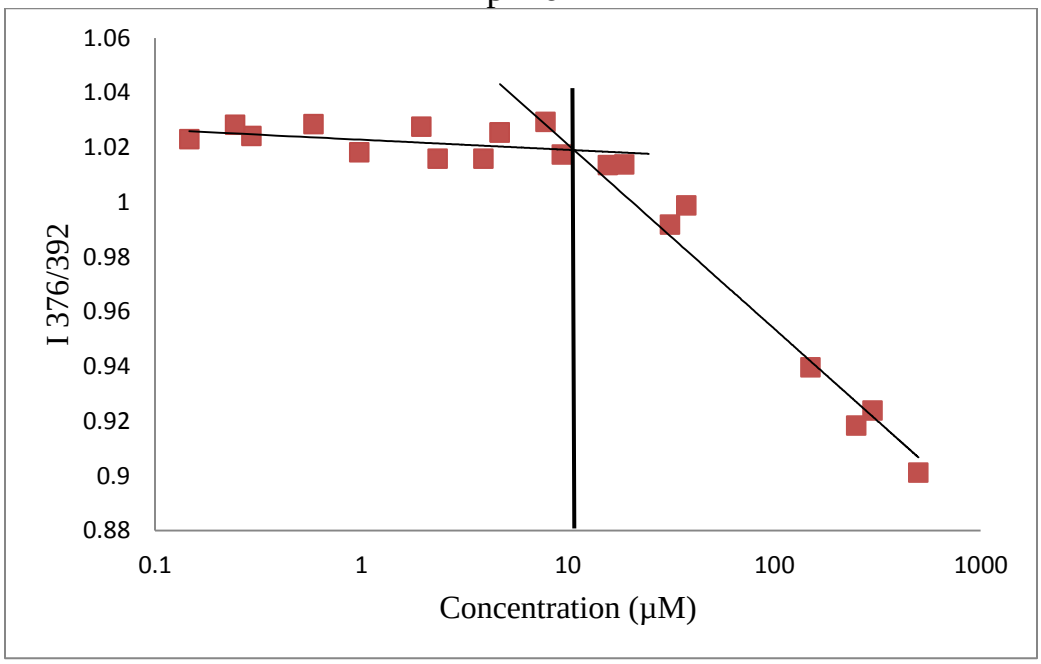

pH 7

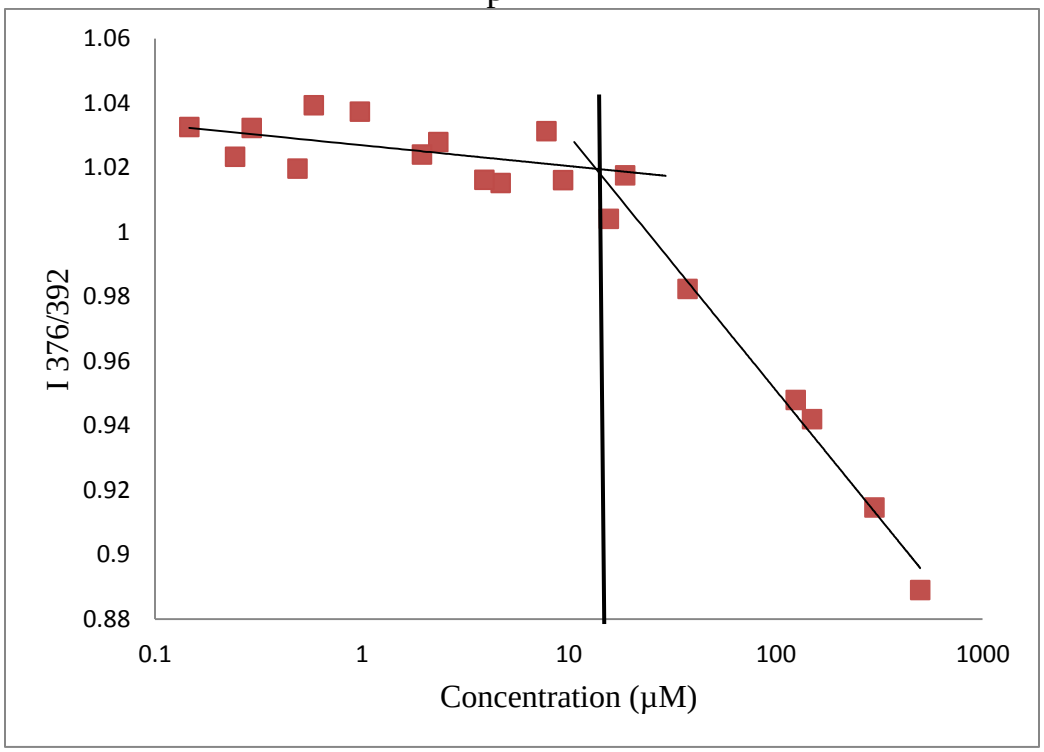
1.06
1.04
1.02
1
0.98
0.96
0.94
0.92
0.9
0.88
I 376/392
0.1
1
10
100
1000
Concentration (µM)

pH 9

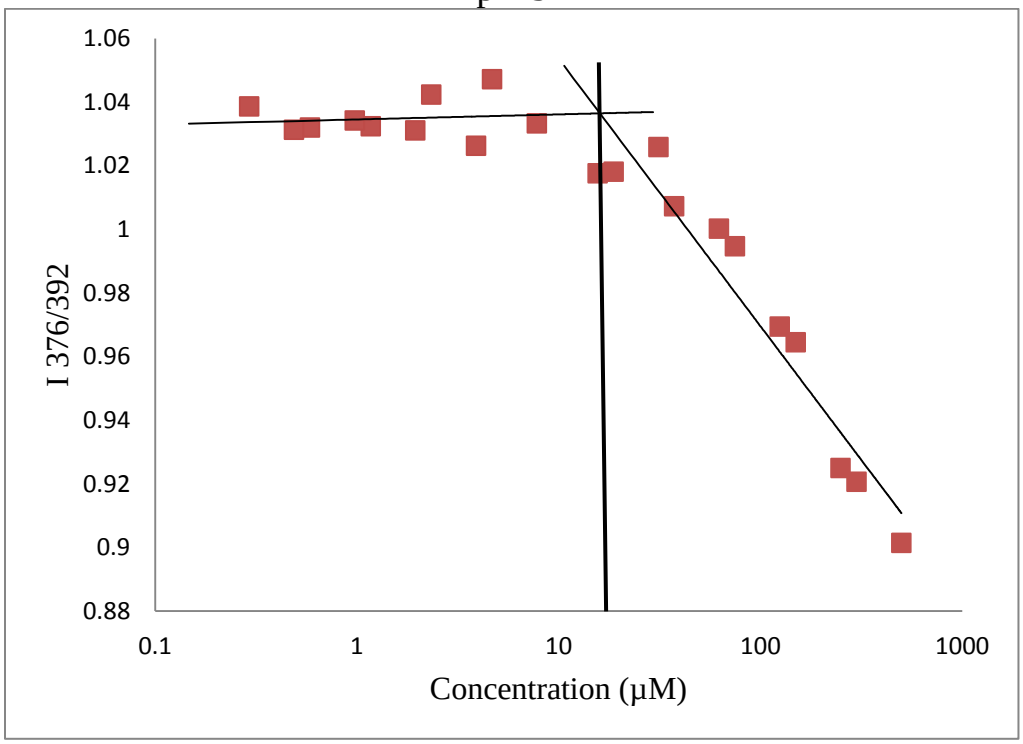
1.06
1.04
1.02
1
0.98
0.96
0.94
0.92
0.9
0.88
I 376/392
0.1
1
10
100
1000
Concentration (µM)

Table of CAC for PA2, PA3, and PA4

pH	PA2 CAC (μM)	PA3 CAC (μM)	PA4 CAC (μM)
5	0	0 (assumed)	7.28
6	5.62	1.18	11.31
7	9.37	3.89	14.08
8	12.58	12.04	
9	21.59	25.47	15.45

Transmission Electron Microscopy:

- PA1 in 150 mM NaCl and 2.2 mM $CaCl_2$

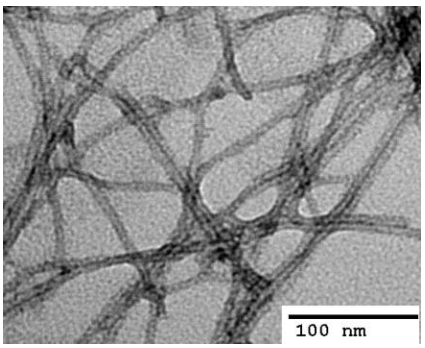

500 μM at pH 5

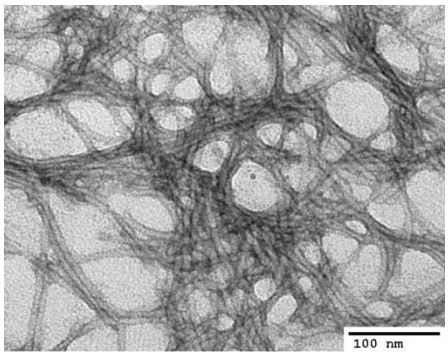

500 μM at pH 10

- PA2 in 150 mM NaCl and 2.2 mM $CaCl_2$

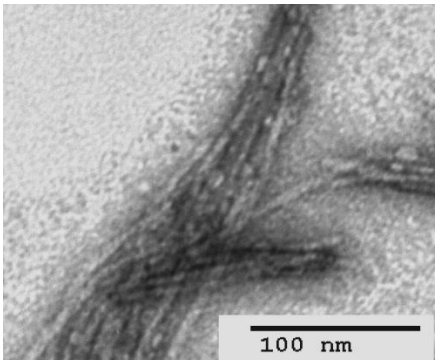

500 μM at pH 5

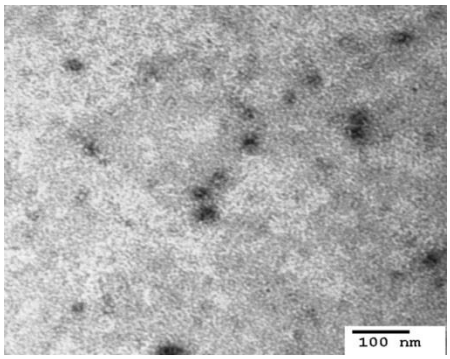

500 μM at pH 9

- PA3 150 mM NaCl and 2.2 mM $CaCl_2$

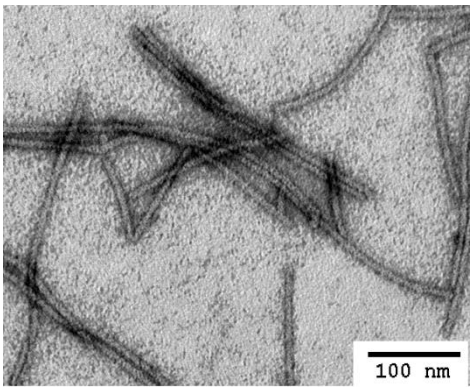

500 μM at pH 5

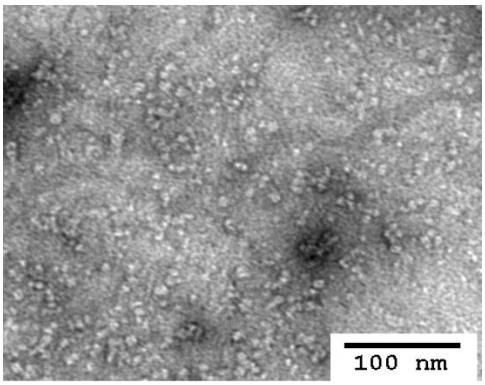

500 μM at 9

References:

(1) "Cancer Statistics" National Cancer Institute. Web. **2012**

(2) "Cancer" World Health Organization. Web. **2014**

(3) Mulvey, J. J., et al; *Nature Nanotechnology*, **2013**, 8, 763-71

(4) Dhanasekaran, S.M., et al; *Nature*, **2001**, 412,822-6

(5) Tomlins, S.A., et al; *Science Translational Medicine*, **2011**, 3 (94), 1-12

(6) Thomas, J.M., et al; *JACS*, **2012**, 134, 13823-33

(7) Gao, X., et al; *Nature Biotechnology*, **2004**, 22 (8), 969-76

(8) Cheetham, A.G., et al; *JACS*, **2013**, 135, 2907-10

(9) Qin, S.Y., et al; *Langmuir*, **2011**, 28, 2083-90

(10) Bartkova, J. et al; *Nature*, **2005**, 434, 864-70

(11) Ganta, S., et al; *Journal of Controlled Release*, **2008**, 126, 187-204

(12) Gatenby, R., et al. *Nature Reviews Cancer*, **2004**, 4 (11), 891-9

(13) Ghosh, A. et al; *JACS*, **2012**, 134 (8), 3647-50

(14) Chauhan, V.P., et al; *Nature Nanotechnology*, **2012**, 7, 383-8

(15) Gullotti, E., et al.; *Molecular Pharmaceutics*, **2009**, 6 (4), 1041-51

(16) Tweedle, M.F.; *Accounts of Chemical Research*, **2009**, 42 (7), 958-68

(17) Dischino, D.D., et al; *Inorganic Chemistry*, **1991**, 30, 1265-9

(18) Preslar, A.T., et al; *ACS Nano*, **2014**, 8 (7), 7325-32

(19) Amblard, M., et al; *Molecular Biotechnology*, **2006**, 33(3), 239-54

(20) Kim, C.A., et al; *Nature Letters*, **1993**, 362, 267-70

(21) Minor, D.L., et al; *Nature Letters*, **1994**, 367, 660-3

(22) Greenfield, N. J.; Nature Protocols, **2006**, 1 (6), 2876-90

(23) Aguiar, J., et al; *Journal of Colloid and Interface Science*, **2003**, 258, 116-22

(24) Greenfield, N. J., et al; *Biochemistry*, 1969, 8 (10), 4108-16